Theor Chem Acc (2015) 134:77
DOI 10.1007/s00214-015-1668-9

REGULAR ARTICLE

Non-covalent attraction of $B_2N^{(-,0)}$ and repulsion of $B_2N^{(+)}$ in the B_nN_n ring: a quantum rotatory due to an external field

Majid Monajjemi[1]

Received: 26 January 2015 / Accepted: 15 April 2015 / Published online: 23 May 2015

Abstract The three radical, anion and cation forms of $B_2N^{(-,0,+)}$ have been studied inside the $B_{12}N_{12}$ ring and compared with one another in terms of non-covalent interaction. Not only does the symmetry breaking (SB) of $B_2N^{(-,0,+)}$ exhibit an energy barrier in the scale of millihartree (10–50) (depending on whether it is in on ionic or neutral forms), but it also create several SBs through the asymmetry stretching and bending mode interactions. We have previously figured out that the double well minimum of the BNB's potential diagram is due to the lack of the proper permutational symmetry of its wave function and charge distribution. In this study, an extreme enhancement in the energy barrier of SB effect was observed upon the interaction of BNB (both radical and cation) with $B_{12}N_{12}$ ring. Such amount was not observed for the isolated BNB structure. Depending on the diameter of B_nN_n and whether the system is ionic or radical, the interaction of $B_2N^{(0,-,+)}$ with the ring is either repulsive or attractive. The $BN^{(-,0,+)}$ B–$B_{12}N_{12}$ system works as a quantum rotatory system, which has a range of spectrum in the IR region due to the alternative attraction and repulsion forces.

Keywords Boron nitride cages · Non-bonded interaction · Hyperfine properties · Dipole moment · ChelpG · EPR-II and III · MESP (EP)

✉ Majid Monajjemi
m_monajjemi@srbiau.ac.ir

[1] Department of Chemistry, Science and Research Branch, Islamic Azad University, Tehran, Iran

1 Introduction

The triatomic BNB structure (i.e., radical, cation and anion) represents one of the most complicated examples of symmetry breaking (SB) effect, which can either be real or artifactual, due to its susceptibility to a pseudo-second-order Jahn–Teller effect. A number of experimental as well as theoretical studies have been devoted to this system [1–12]; however, there are no reports on the SB of ionic structures in a non-covalent interaction with B_nN_n rings (except for a brief study in our previous works) [13–16].

The first major study on the B_mN_{3-m} ($m = 0, 1, 2$ and 3) was carried out by Martin et al. [1]. The UHF/6-31G* geometry optimization results have predicted the asymmetric linear arrangement of the B_2N in its ground state with an extremely low bending frequency of 73 cm^{-1} [1].

In general, the researchers are in agreement with the linearity of BNB in its ground electronic state of $(\tilde{X}^1\sum_g^+)$ and $(\tilde{X}^2\sum_u^+)$ in its ionic and neutral forms. The ground state of the $BN^{(0)}B$ radical has been examined via the developed reduced multireference coupled-cluster method with singles and doubles that is perturbatively corrected for triples [RMR CCSD(T)] using the correlation consistent basis sets (cc-pV*DZ*, cc-pV*TZ* and cc-pV*QZ*) by Paldus [9].

Similar to earlier results that were based on the single reference CCSD (T) and BD (T) approaches, the RMR CCSD (T) method also predicts an asymmetric structure with two BN bonds of unequal length, even though the MR effects would result in a significantly reduced barrier height.

The state of $\tilde{A}^2\sum_g^+(B_2N^-)$ was observed in photoelectron spectroscopic studies (PES), placing the zero-point level of the 6330 ± 40 cm^{-1} above the ground state of the

$\tilde{X}^2\sum_u^+$ by Asmis [2]. He exhibited that the signal observed in the 355 and 266 nm photoelectron spectra of B_2N^- has been indicated to a photo detachment from the anion ground state $(\tilde{X}^1\sum_g^+)$ to the ground and lowest excited state of neutral B_2N $\{(\tilde{X}^2\sum_u^+)$ and $(\tilde{A}^2\sum_g^+)\}$ with a linear symmetry and assigned to the $\tilde{X}^1\sum_g^+ \rightarrow \tilde{X}^2\sum_u^+ + e^-$ and $\tilde{X}^1\sum_g^+ \rightarrow \tilde{A}^2\sum_g^+ + e^-$ transitions. Furthermore, the infrared absorptions were also observed in the cryogenic argon matrix near 6000 $cm^{-1}$of electronic band system, due to the $\tilde{A}^2\sum_g^+ — \tilde{X}^2\sum_u^+$ [7].

It appears that Walsh's prediction [17] of linear *p*-block molecules is holding up quite well for all $BN^{(-,0,+)}$ ions and BNB radical would be the first of the 11 valence electron structures which upon adding an additional electron would change to the ground electronic configuration from $\left(\tilde{X}^2\sum_u^+\right)$ to $\left(\tilde{X}^1\sum_g^+\right)$ for $B_2N^{(0)}$ and B_2N^-, respectively.

We have previously shown that some of the B_nN_n rings such as $B_{18}N_{18}$, $B_{15}N_{15}$ and $B_{12}N_{12}$ are in suitable position in order to generate a stable system of non-bonded interaction between the rings and linear molecules of $BN^{(-,0,+)}B$ [15].

The combination of the rings and $BN^{(-,0,+)}B$ ion molecules enables us to resolve the controversy of the geometry of B_2N in viewpoint of real or artifactual symmetry breaking of BNB, and the concept of non-bonded interaction in ground and exited states of B_nN_n–BNB systems.

In this study, we have observed that the energy barrier of SB for BNB (both radical and cation) upon its interaction with $B_{12}N_{12}$ increases dramatically. In other words, the external field of $B_{12}N_{12}$ would result in a stronger pseudo-second-order Jahn–Teller effect.

To answer for this phenomenon, we have investigated the quantum mechanics of non-bonded interaction in terms of wave function and charge density.

In addition, although the total wave function of each molecule in our system (for Φ_n^{BNB} and $\Phi_m^{B_{12}N_{12}}$) under the permutation of electron coordinates is anti-symmetric, the product states of these non-bonded molecules under intermolecular exchange of the electrons cannot be anti-symmetric.

An obvious solution to this would be to introduce the intermolecular anti-symmetrizer operator "$\tilde{A}$". However, this would result in two major problems which have been shown by Eisenschitz [18–20], that is, the anti-symmetrized unperturbed states are no longer eigen-functions of $H^{(0)}$, which are followed by the $\left[\tilde{A}, H^{(0)}\right] \neq 0$, where the projected excited states, $\tilde{A}^{BNB-B_{12}N_{12}B}\Phi_n^{BNB}\Phi_m^{B_{12}N_{12}}$, become linearly dependent [18–21] and the choice of a linearly independent subset is not apparent.

The first-order energy including exchange can be written as:

$$E^{(1)}_{\text{antisymm}} = \frac{\left\langle \Phi_0^{BNB}\Phi_0^{B_{12}N_{12}} \middle| V^{BNBB_{12}N_{12}}\tilde{A}^{BNBB_{12}N_{12}} \middle| \Phi_0^{BNB}\Phi_0^{B_{12}N_{12}} \right\rangle}{\left\langle \Phi_0^{BNB}\Phi_0^{B_{12}N_{12}} \middle| \tilde{A}^{BNBB_{12}N_{12}} \middle| \Phi_0^{BNB}\Phi_0^{BB_{12}N_{12}} \right\rangle} \tag{1}$$

Although the exchange interaction is commensurate to the differential overlap between two parts, in practice, it was difficult to apply *those energies*. As a consequence, exchange interactions between BNB molecule and $B_{12}N_{12}$ ring have been neglected.

The wave functions as well as the exchange interaction fade exponentially as a function of distance [18–21]. Therefore, a B_nN_n ring with a small diameter has been considered in our model of non-bonded system due to suitable overlapping (the exchange interactions are neglected).

In the case of chemical bonding, this interaction is always attractive; though, in the case of intermolecular forces, the interaction is repulsive or attractive depending on ionic or radical situation as well as the diameter of B_nN_n rings.

The RS-PT theory [18–25] (without exchange) is applied to two parts of BNB and $B_{12}N_{12}$ structures. One part uses the unperturbed Hamiltonian, and the other part uses the sum of two monomer Hamiltonians, i.e., $H^{(0)} \equiv H^{BNB} + H^{B_{12}N_{12}}$.

In the present case, the unperturbed states are produced, i.e., $\Phi_n^{BNB}\Phi_m^{B_{12}N_{12}}$ with $H^{BNB}\Phi_n^{BNB} = E_n^{BNB}\Phi_n^{BNB}$ and $H^{B_{12}N_{12}}\Phi_n^{B_{12}N_{12}} = E_n^{B_{12}N_{12}}\Phi_n^{B_{12}N_{12}}$

$$E^{(1)}_{\text{electrostatic}} = \left\langle \Phi_0^{BNB}\Phi_0^{B_{12}N_{12}} \middle| V^{BNBB_{12}N_{12}} \middle| \Phi_0^{BNB}\Phi_0^{B_{12}N_{12}} \right\rangle \tag{2}$$

The total charge density of BNB is given by:

$$\rho^{BNB}_{\text{tot}(r)} = \sum_{\alpha_i} z_{\alpha_i}\delta(r - R_{\alpha_i}) - \rho^{BNB}_{el}(r) \tag{3}$$

which α_i is the nucleus of B and N and has position vector $\mathbf{R}\alpha_i$, then its charge times the Dirac delta function, Z_α $\delta(\boldsymbol{r} - \mathbf{R}\alpha_i)$, is the charge density of these nuclei.

And the electronic charge density is given by an integral over $n - 1$ electron coordinates of BNB ions as follows:

$$\rho^{BNB}_{\text{el}}(r) = n\int \left|\Phi_0^{BNB}\left(r, r_2', r_3', \ldots r_n'\right)\right|^2 \mathrm{d}r_2', \mathrm{d}r_3' \ldots \mathrm{d}r_n' \tag{4}$$

It can be shown that the first-order quantum mechanical expression can be written as:

$$E^{(1)}_{\text{electrostatic}} = \iint \rho^{BNB}_{\text{tot}}(r_1)\frac{1}{r_{12}}\rho^{B_{12}N_{12}}_{\text{tot}}(r_2)\mathrm{d}r_1\mathrm{d}r_2 \tag{5}$$

This indicates that the first-order RS-PT energy is indeed equal to the electrostatic interaction between *BNB* and $B_{12}N_{12}$, which has been used in this study $\{\Delta E = E_{B_{12}N_{12}-BNB} - (E_{B_{12}N_{12}} + E_{BNB})\}$. It is obvious that the relative motion of the nuclei including vibration and rotation with non-bonded system of $B_{12}N_{12}$–$B_2N^{(-,0,+)}$ affects the electron density of both the ground and exited states with the electronic structures of $B_2N^{(-,0,+)}$.

We have investigated the ion–dipole and dipole–dipole interaction of two non-overlapping parts of $BN^{(-,0,+)}B$ and $B_{12}N_{12}$ in terms of electronic structures of BNB. In the case of ionic structure, it can be argued that the ionic–dipole interactions between $B_{12}N_{12}$ and $BN^{(-,+)}B$ are seen as either intermolecular forces or a rather special kind of force where the interaction between them can be seen as a special case of multipolar attraction, which is inversely proportional to the power of the distance $\left(\frac{1}{R_{AB}^n}\right)$.

The results indicate that in the ground state, there is an attraction between $\left(BN^{(-,0)}B\right)$ and $(B_{12}N_{12})$, while there is a repulsion between $\left(BN^{(+)}B\right)$ and $(B_{12}N_{12})$. In the exited state of BNB on the other hand, all interactions between the two structures are attraction.

Due to the molecular free rotation in the neutral form of $BN^{(0)}B$, the total electrostatic interaction energy for the dipole–dipole interaction becomes zero (it is evidently [26] much weaker than the un-averaged one, but it is not exactly zero).[1] The total electrostatic interaction energy of our system is considered ($U_{B_{12}N_{12}-BNB}$) between two charge distributions as it is indicated in Eq. 4:

$$U_{B_{12}N_{12}-BNB} = \sum_{\mu\in B_{12}N_{12}} \sum_{\nu\in BNB} \frac{q_\mu q_\nu}{r_{\mu\nu}} \tag{6}$$

Because of the electrostatic interaction between $B_{12}N_{12}$ and BNB, the charge distribution of $B_2N^{(-,0,+)}$ molecule in the $B_{12}N_{12}$ ring polarizes the charge distribution and induces electromagnetic field of the $B_{12}N_{12}$–BNB systems. This is followed by the appearance of a dipole moment, which is a result of an electric charge distribution. The Hamiltonian with consideration of BO approximation for two non-bonded systems of $B_{12}N_{12}$ and B_2N can be written as:

$$H^{(\text{Non}-\text{bonded})} = H^{B_{12}N_{12}} + H^{B_2N} \tag{7}$$

where the unperturbed states are products $\Phi_k^{B_{12}N_{12}}\Phi_m^{\{B_2N\}}$ with

$$H^{\{B_{12}N_{12}\}}\Phi_k^{B_{12}N_{12}} = E_k^{B_{12}N_{12}}\Phi_k^{B_{12}N_{12}} \tag{8}$$

and

$$H^{B_2N}\Phi_m^{B_2N} = E_m^{B_2N}\Phi_m^{B_2N} \tag{9}$$

It is currently possible to calculate the electrostatic energy of the molecule without any further approximations other than those applied in the calculation of the monomer's wave functions using a multipole expansion for the electrostatic energy [27–30].

2 The interactions between $B_{12}N_{12}$ and BNB

Scheme 1 indicates the structure of BNB and $B_{12}N_{12}$ molecules at distance R (from the BNB to each loop or each B–N bond of $B_{12}N_{12}$), considering that their wave functions' overlapping is too small that it can be neglected. Particles $i \in$ BNB and $j \in B_{12}N_{12}$ are assumed in our model in Scheme 2.

The total Hamiltonian $H = H^{(0)} + H^{(1)}$ consists of two parts: (A) free molecule of $H^{(0)} = H^{B_{12}N_{12}} + H^{BNB}$ and (B) interaction operator of $H^{(1)} = \sum_{i\in BNB}\sum_{j\in B_{12}N_{12}} \frac{q_i q_j}{r_{ij}}$.

The loops and B–N bonds of $B_{12}N_{12}$ ring provide an external potential "$V_{(ri)}$" for $BN^{(-,0,+)}B$ which is $V_{(r_i)} = \sum_{j\in B_{12}N_{12}} \frac{q_j}{r_{ij}}$; thus, we have: $H^{(1)} = \sum_{i=1}^n q_i V(r_i) = \sum_{i=1}^n q_i V(x_i, y_i, z_i)$.

Substituting into the $H^{(1)}$ after some rearrangements results in Eq. 10:

$$\begin{aligned} H^{(1)} = & \frac{\sum_{(i=1)\in BNB}^n \boldsymbol{q_i} \sum_{(j=1)\in B_{12}N_{12}}^n \boldsymbol{q_j}}{R} \\ & + \frac{\sum_{(i\in BNB)}^n \boldsymbol{q_i r_i} q^{B_{12}N_{12}}}{R^2} - \frac{\sum_{(j\in BNB)}^n \boldsymbol{q_j r_j} q^{BNB}}{R^2} \\ & + \frac{\mu_x^{BNB}\mu_x^{B_{12}N_{12}} + \mu_y^{BNB}\mu_y^{B_{12}N_{12}} - 2\mu_z^{BNB}\mu_z^{B_{12}N_{12}}}{R^3} \end{aligned} \tag{10}$$

where the total charges are equal to $q^{BNB} = \sum_{(i=1)\in BNB}^n q_i$, $q^{B_{12}N_{12}} = \sum_{(j=1)\in B_{12}N_{12}}^n q_j$ (and the dipole operators are $\mu^{BNB} = \sum_{(i=1)\in BNB}^n q_i r_i, \mu^{B_{12}N_{12}} = \sum_{(j=1)\in B_{12}N_{12}}^n q_j r_j$.

The operator $H^{(1)}$ includes the electrostatic interactions between the charges and dipole moments of BNB and $B_{12}N_{12}$ molecules (including four loops and four B–N bonds).

The interaction tensor's operator can be used as an alternative form of the dipole–dipole interaction operator as follows:

$$\begin{aligned} & \frac{\mu_x^{BNB}\mu_x^{B_{12}N_{12}} + \mu_y^{BNB}\mu_y^{B_{12}N_{12}} - 2\mu_z^{BNB}\mu_z^{BB_{12}N_{12}}}{R^3} \\ & = \frac{\mu^{BNB}\mu^{B_{12}N_{12}} - 3\mu_z^{BNB}\mu_z^{B_{12}N_{12}}}{R^3} = \frac{\mu^{BNB}\cdot\hat{\boldsymbol{T}}\cdot\mu^{B_{12}N_{12}}}{R^3} \end{aligned} \tag{11}$$

[1] It was first shown by John Lennard-Jones [26] that the temperature-averaged dipole–dipole interaction is $\bar{E}_{dip-dip} = -\frac{2kT}{3R_{AB}^6}\mu_A^2\mu_B^2$, since averaged energy has R^{-6} dependence.

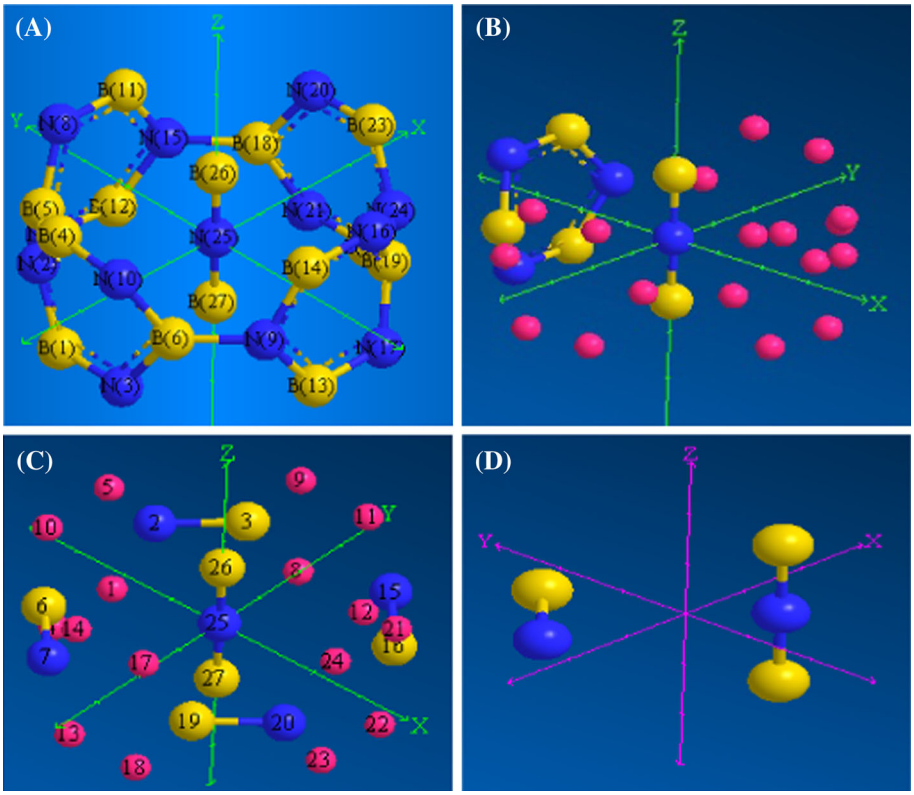

Scheme 1 The BNB structure in interaction with B–N bonds of $B_{12}N_{12}$ ring in four different configurations: **a** full fragment of the ring, **b**, **c** considering some of the atoms as dummy atoms, and **d** only the B–N with all other atoms as dummy atoms

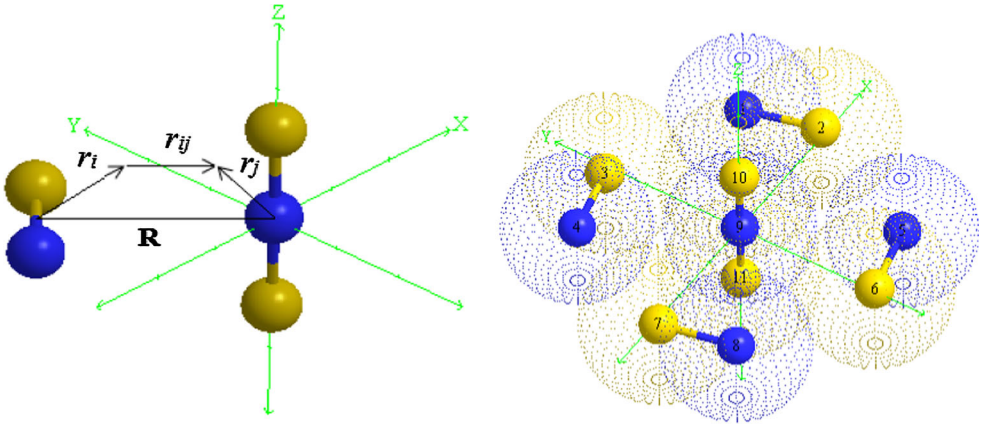

Scheme 2 The BNB and $B_{12}N_{12}$ structures at distance R from the BNB to each B–N bond of particles: $i \in$ BNB and $j \in B_{12}N_{12}$, $r_i = (x_i, y_i, z_i)$ and $r_j = (x_j, y_j, z_j)$, $\mathbf{R} = (0, 0, R)$, $r_{ij} = r_j - r_i + R$

With the interaction tensor $\hat{\boldsymbol{T}} = \begin{bmatrix} T_{xx} & T_{yy} & T_{zz} \\ T_{yx} & T_{yy} & T_{yz} \\ T_{zx} & T_{zy} & T_{zz} \end{bmatrix} = \begin{bmatrix} 1 & 0 & 0 \\ 0 & 1 & 0 \\ 0 & 0 & -2 \end{bmatrix}$, this can also be expressed in more general coordinates.

The solutions of the Schrödinger equations of the isolated BNB and $B_{12}N_{12}$ molecules are: $H^{\mathrm{BNB}}\Phi_{K_1}^{\mathrm{BNB}} = E_{K_1}^{\mathrm{BNB}}\Phi_{K_1}^{\mathrm{BNB}}$ and $H^{\mathrm{B_{12}N_{12}}}\Phi_{K_1}^{\mathrm{B_{12}N_{12}}} = E_{K_1}^{\mathrm{B_{12}N_{12}}}\Phi_{K_1}^{\mathrm{B_{12}N_{12}}}$ and the eigenvalues of unperturbed terms $(H^{(0)}\Phi_K^{(0)} = E_K^{(0)}\Phi_K^{(0)}$ with $\Phi_K^{(0)} = \Phi_{K_1}^{\mathrm{BNB}}\Phi_{K_2}^{\mathrm{B_{12}N_{12}}})$ are $E_K^{(0)} = E_{K_1}^{A} + E_{K_2}^{B}$.

Therefore, the first-order energy can be indicated as in Eq. 10:

$$E_0^{(1)} = \left\langle \Phi_0^{(0)} \middle| H^{(1)} \middle| \Phi_0^{(0)} \right\rangle = \left\langle \Phi_0^{A\mathrm{BNB}}\Phi_0^{B\mathrm{B_{12}N_{12}}} \middle| H^{(1)} \middle| \Phi_0^{\mathrm{BNB}}\Phi_0^{\mathrm{B_{12}N_{12}}} \right\rangle. \quad (12)$$

Including the multipole expansion of $H^{(1)}$, whose integration can be separated over the coordinates (x_i, y_i, z_i) and (x_j, y_j, z_j) of the particles $i \in$ BNB and $j \in B_{12}N_{12}$, while the permanent multipole moments are $\langle \mu^{\mathrm{BNB}} \rangle = \langle \Phi_0^{\mathrm{BNB}} | \mu^{\mathrm{BNB}} | \Phi_0^{\mathrm{BNB}} \rangle$ and $\langle \mu^{\mathrm{B_{12}N_{12}}} \rangle = \langle \Phi_0^{\mathrm{B_{12}N_{12}}} | \mu^{\mathrm{B_{12}N_{12}}} | \Phi_0^{\mathrm{B_{12}N_{12}}} \rangle$.

The second-order energy is:

$$E_0^{(2)} = \sum_{k\neq 0} \frac{\left\langle \Phi_0^{(0)} \middle| H^{(1)} \middle| \Phi_K^{(0)} \right\rangle \left\langle \Phi_K^{(0)} \middle| H^{(1)} \middle| \Phi_0^{(0)} \right\rangle}{E_0^{(0)} - E_k^{(0)}} \quad (13)$$

where the index k that labels the excited states of the system is a composite index: $k = (k_1, K_2)$. The summation over $k \neq 0$ can split into three sums, with $k_1 \neq 0$ and $K_2 = 0$ for BNB excited molecule, $k_2 \neq 0$ and $k_1 = 0$ for $B_{12}N_{12}$ excited molecule, and $k_1, k_2 \neq 0$ for both excited molecules. In our systems, we assume the $B_{12}N_{12}$ is in ground state, and only, the $BN^{(-,0,+)}B$ can be exited to higher levels of energy.

The major point is to investigate the electrostatic interaction of BNB with the $B_{12}N_{12}$ ring surrounding it, which can form the basis for more detailed studies of other non-bonded interacting systems.

In order to investigate the electrostatic interactions of the BNB with four different segments, including four loops and four connecting bonds of $B_{12}N_{12}$ ring within vertical transition, first the three loops have been frozen and the electrostatic interaction of BNB with the one remaining active loop has been taken into account (Schemes 1, 2).

Other loops have been examined one by one in the same way, and the changes of all the following calculated quantities have been explored. We then focused on each bond of $B_{12}N_{12}$ individually and evaluated the interaction of BNB with each of the four connecting bonds of $B_{12}N_{12}$ ring and repeated the calculations along each bond [14].

Based on previous studies [13–15], the dipole expansions are used in the study of electromagnetic fields of charge and current distributions. It is only for the clustered system with large density fluctuation that such a fast method has a superior efficiency [27–30]. Therefore, the lack of experimental demonstration and its importance in theoretical simulations was a motivation for us to investigate dipole moments from theoretical point of view.

The coefficients of angular coordinates of multipole moment are defined as a sum of spherical harmonics $\left[f(\theta,\varphi) = \sum_{l=0}^{\infty} \sum_{m=-l}^{l} C_l^m Y_l^m(\theta,\varphi)\right]$. The total electrostatic interaction energy of the system is taken into consideration $(U_{B_{12}N_{12}-BNB})$ between the two charge distributions from Eq. 6.

Due to the electrostatic interaction between $B_{12}N_{12}$ and BNB, the charge distribution of $B_{12}N_{12}$ ring gets polarized by BNB inside the ring and the electromagnetic field in the $B_{12}N_{12}$–BNB system gets induced.

The dipole moment which has appeared due to an electric charge distribution usually involves powers (or inverse powers) of the distance of the origin (r) as well as some angular dependence (Θ and ϕ). The dipole moment is converged under two conditions: (1) for the charges which are localized close to the origin and to the point where the observed potential is far from the origin of which the coefficients of the expansion series are called exterior dipole moments or simply dipole moments and (2) for the charges which are located far from the origin and the observed potential close to the origin, namely interior dipole moments.

The importance of this quantity is due to the fact that the potential at a position within a charge distribution can often be computed by combining interior and exterior dipoles [14, 27–30].

When only a single BNB molecule is considered, $\Theta = \phi = 0$, i.e., the dipole vector would be coincided with the BNB axis. According to the obtained dipole moments, it can be distinguished that the r component of the dipole moment vector of each cationic and anionic radical forms of BNB which are involved in the ring had the tendency to rotate in three different conical surfaces.

So, it could be realized that our observed dipole moment has been directed linearly and this observation supported the intrinsic linear form of BNB molecule.

In this regard, it seems that if an extrinsic factor (such as a biomolecules) is set in the BNB–$B_{12}N_{12}$ system due to generation of radical, anion and cation forms of BNB, the electrical current will cross along the ring that changes all calculated atomic physico-chemical properties.

Here, it is notable that the three emerged radical, cationic and anionic forms of BNB generate frequently to each other, and if these three species are imagined in the three quantized cone surfaces, it can be deduced that the variation of the radial vector of dipole moment (r) of the system would be quantized when crossing these three cone levels [14].

An induced dipole of any polarizable charge distribution ρ of the BNB molecule is caused by an electric field external to ρ that originates from an ion or polar molecule in the vicinity of ρ.

The strength of the induced dipole is equal to the product of the strength of the external field and the dipole polarizability of ρ. So, along with the variation of the radial component, (r) the two other remaining components of the dipole moment, namely Θ and ϕ, will be changed and cause the quantized rotation of BNB molecule. Due to the electrical charge of BNB and its induced electrostatic interaction, the ring will be affected and the rotation of $B_{12}N_{12}$ ring is also expected to be quantized.

3 Computational details

The calculation has been done for the isolated system of BNB by the CASSCF (10, 12) level of methods including EPR-II, EPR-III and AUG-cc-pvqz level of basis sets. For

the radical systems, we have considered the UHF and ROHF.

The energy of $B_2N^{(-,0,+)}$ in ground and exited states inside the $B_{12}N_{12}$ ring has been done via various methods such as M062x/6-31g*, M062x/EPR-II, B3p86/EPR-ii, B3p86/6-31g* and B3LYP/6-31g*.

The $B_{12}N_{12}$ system has been optimized via the CASSCF (10, 12) level of methods and EPR-II, EPR-III and AUG-cc-pvqz level of basis sets.

The charges from "ECP fitting" have been calculated via QCISD/EPR-III, m062x/6-31g, b3p86/6-31g, HF/EPR-ii, HF/6-31g* and m062x/EPR-ii for $BNB^{(-,0,+)}$ in both positions of isolated and external field of $B_{12}N_{12}$.

Attraction and repulsion energies between $BNB^{(-,0,+)}$ and $B_{12}N_{12}$ ring in ground and exited states have been done via:

UHF/EPR-ii ($r_e = 1.3105$), M062x/EPR-ii ($r_e = 1.335$), UHF/6-31g*($r_e = 1.3089$), HF/6-31g*($r_e = 1.302$), B3P86/6-31g*($r_e = 1.3198$), M062x/6-31g*($r_e = 1.3208$), HF/6-31g*($r_e = 1.3371$), B3LYP/6-31g*//QCISD(T)/EPR-iii ($r_e = 1.3079$), B3LYP/6-31g*//QCISD(T)/EPR-iii ($r_e = 1.3422$), B3LYP/6-31g*//QCISD (T)/EPR-iii ($r_e = 1.2976$) and B3p86/EPR-ii//CASSCF (11,12) ROHF/AUG-cc-PVQZ ($r_e = 1.294$), where the "r_e" is the equilibrium bond length for the isolated BNB in three forms of anion, radical and cation in different levels of theory.

Among the various methods and basis sets (both large and medium) which have been used in this study, the EPR-III and EPR-II basis sets of Barone [31] show the most favorable results for electrostatic potential (ESP) fitting. The EPR-II is a double-ζ basis set with a single set of polarization functions for B to F [32, 33]. EPR-III is a triple-ζ basis set including diffuse functions, double d-polarizations and a single set of polarization functions. In the latter case, the s-part is also improved to better describe the nuclear region for B to F [31–34].

The active space for the CASSCF method was composed of all valence electrons and orbitals of these atoms, i.e., 11 active electrons and 12 active orbitals for $B_2N^{(0)}$ and 10 and 12 electrons for $B_2N^{(+)}$and $B_2N^{(-)}$, respectively. In some part of our discussion, the BNB has been optimized via various levels of theory such as CASSCF (11, 12)/cc-pvqz and CASSCF (11, 12)/AUG-cc-pvqz (for radical) and CASSCF (10, 12)/cc-pvqz for cation. Approximate spin orbit coupling between two spin states has also been taken into account during CASSCF calculations [35, 36].

A quadratic CI calculation including single and double substitutions [37] has been used to evaluate various one-electron properties including NBO, bonding analysis, atoms in molecules (AIM) [38], natural population analysis, multipole moment, electrostatic potentials and electrostatic potential-derived charge using the Merz–Kollman–Singh [39], chelp [40] or chelpG [41].

Polarizabilities and hyper-polarizabilities have been computed by CISD and QCISD and CASSCF methods and double numerical differentiation of energies have been used by pol = En only keyword in some cases. The AIM keyword is used to compute atomic charges of atoms in molecules, covalent bonds, localized orbitals and critical points, and the properties have been used to request molecular properties predicted via theory of atoms in molecules [38]. Atomic charges have been calculated from electrostatic potentials using a grid-based method, ChelpG, which is developed by Breneman and Wiberg [41].[2] Atomic charges are fitted to reproduce the molecular electrostatic potential (MESP) at a number of points around the molecule.[3] The charge calculation methods based on molecular electrostatic potential (MESP) fitting are not well suited for treating larger systems where some of the innermost atoms are located far away from the points at which the MESP is computed. In such a condition, variations of the innermost atomic charges will not lead to significant changes of the MESP outside of the molecule, meaning that the accurate values for the innermost atomic charges are not well determined by MESP outside of the molecule.

The representative atomic charges for molecules should be computed as average values over several molecular conformations. A detailed overview of the effects of the basis set and the Hamiltonian on the charge distribution can be found in [42]. CHELPG charges can be computed using the well-known ab initio quantum chemical packages such as Gaussian or GAMESS-US.

In this study, it is indeed difficult and at some points not necessary to use large basis sets and demanding methods such as MRCI for CHELPG and ESP calculations due to the large number of calculations in various situations of MESP simulation. Therefore, with medium methods in terms of computational cost, we have found the accurate results for our approach. All the calculations were performed using the Gaussian program package [43], and the optimization was done along with a frequency calculation

[2] An improved method for computing potential-derived charges is described which is used upon the CHELP program available from QCPE. This approach (CHELPG) is shown to be considerably less dependent upon molecular orientation than the original CHELP program. The results are compared to those obtained by using CHELP.

[3] In the CHELPG (charges from electrostatic potentials using a grid-based method), atomic charges are fitted to reproduce the molecular electrostatic potential (MESP) at a number of points around the molecule. The MESP is calculated at a number of grid points spaced 3.0 pm apart and distributed regularly in a cube. Charges derived in this way do not necessarily reproduce the dipole moment of the molecule. CHELPG charges are frequently considered superior to Mulliken charges as they depend much less on the underlying theoretical method used to compute the wave function (and thus the MESP).

to verify that the geometry was a real minimum without any imaginary frequency.

4 Results and discussion

The discussion has been categorized in the three split-level subsections dealing with (a) structural aspects, (b) energetic aspects and (c) calculation of properties.

Consequently, the results for the structure and energies are listed in the Tables 1, 2 and 3. The data for the attraction and repulsion energies (eV) between $BNB^{(-,0,+)}$ and $B_{12}N_{12}$ ring (in the ground and exited states) are listed in Table 4. The calculated physical parameters of the isolated and non-isolated forms of $B_2N^{(-,0,+)}$ in the ground and exited states are listed in Tables 5 and 6.

4.1 Structural aspects

Radical form of BNB is linear in its ground electronic state $\left(\tilde{X}^2\sum_u^+\right)$ with an orbital occupancy of $1\sigma_g^2, 1\sigma_u^2, 2\sigma_g^2, 3\sigma_g^2, 2\sigma_u^2, 1\pi_u^4, 4\sigma_g^2, 3\sigma_u^1$ while the lowest electronically excited state is predicted to be $\tilde{A}^2\sum_g^+$, with an orbital occupancy of $1\sigma_g^2, 1\sigma_u^2, 2\sigma_g^2, 3\sigma_g^2, 2\sigma_u^2, 1\pi_u^4, 4\sigma_g^1, 3\sigma_u^2$.

Furthermore, $\tilde{B}^2\Pi_g$ exited state with an orbital occupancy of $1\sigma_g^2, 1\sigma_u^2, 2\sigma_g^2, 3\sigma_g^2, 2\sigma_u^2, \pi_u^4, 4\sigma_g^2, 1\pi_g^1$ (above the $\tilde{A}^2\sum_g^+$) is subject to the Renner–Teller effect, and further exited state depends on the $\left({}^4\Pi_g\right)$ of triplet form.

As it is shown in Figs. 1 and 2, based on Knight's reports [4] [in which the variation of energy with bond angle for finding a minimum around ($''100°$) has been discussed], a cyclic radical or anion $B_2N^{(-,0)}$ in our calculations has not been observed, though, for cation, there is a bulge in the curve at 90° in MP_4DQ and MP_4DSQ methods, which indicates a cyclic B_2N^+. At the SCF level, the lowest energy corresponds to a bent molecule with an angle of 100°; however, for the QCISD (T), MP_4DQ, MP_4DSQ and HF/aug-cc-pVTZ calculations (Fig. 2), the linear structure clearly has the lowest energies for radical and anion structures. Martin [7] has shown a cyclic B_2N ($^2B_2$) via reactions of pulsed laser produced boron and nitrogen atoms in a condensed argon stream (at higher laser power reactions) and has discussed that the vibration of 882.3 cm^{-1} must be considerably an-harmonic.

In the viewpoint of wave function when the isolated BNB has $D_{\infty h}$ symmetry, the real wave function should convert as an irreducible representation of the $D_{\infty h}$ point group. However, "$4\sigma_g^2$" and "$3\sigma_u^1$" become close to degenerate when the two B–N bonds are asymmetrically stretched (while 6σ and 7σ MOs have the same symmetry). So, the excited state of $[\text{core}]6\sigma, 7$ has a rather strong interaction with single and triple excitations. This phenomenon for non-isolated system increases significantly (Table 4). It is obvious that the approximate electronic structure methods could suffer from an artifactual symmetry breaking effect, which would, therefore, be challenged by a real Jahn–Teller distortion. The energy of these distortions for non-isolated form of BNB compared to that of isolated form has two characteristics, (1) high distortion energy and (2) irregular symmetry breaking (Table 4; Figs. 3, 4).

Overall, we are trying to understand the difference between the electromagnetic structures of the BNB when it is isolated compare to that when it is inside the $B_{12}N_{12}$ ring. In the $D_{\infty h}$ symmetry of BNB (isolated system), the unpaired electron is delocalized, while in the asymmetric $C_{\infty v}$ geometry, it is localized on either one of the B atoms. Structures with broken symmetry, $C_{\infty v}$, will be stabilized by this interaction relative to the symmetric $D_{\infty h}$ geometry.

Physically, the second-order Jahn–Teller interaction permits the unpaired electron to localize on a single boron atom, rather than being delocalized. The other two, which correspond to localizing the unpaired electron on one or both of the boron atoms (when the bond lengths are unequal), do not transform as an irreducible representation of $D_{\infty h}$ for BNB radical via any changing of charges on N and either one of the B atoms (Table 1; Fig. 1a, b).

One cannot easily say that the unpaired electron of non-isolated BNB in the symmetry of $D_{\infty h}$ is delocalized since they are under the influence of the external field of $B_{12}N_{12}$. However, it is localized in the asymmetric $C_{\infty v}$ geometry for both isolated and non-isolated forms of BNB. On the other hand, there is a limitation for the unpaired electron of non-isolated BNB to get delocalized, rather than being localized on a single boron atom between two states of $D_{\infty h}$ and $C_{\infty v}$ symmetries. These limitations between localized and non-localized situations for unpaired electron result in enhancement of the symmetry breaking effect of the BNB in a non-bonded interaction state.

4.2 Energetic aspects

In this study, our focus is on getting the results from DFT methods such as b3p86, b3lyp, m062x, m06-L and m06 for the non-bonded interaction between $BNB^{(-,0,+)}$ and $B_{12}N_{12}$, which are monotonous through the comparison between different situations. The m062x, m06-L and m06-HF are new methods with a good correspondence in non-bonded calculations and are useful for the energies according to the distance between two fragments in a molecule with medium ($\sim$2–5 Å) and long ranges ($\geq$5 Å) [44]. For a non-covalent interaction, B3LYP is unable to describe van der Waals [44, 45] complexes, which are bond by medium-range interactions such as the interactions of $B_{12}N_{12}$–BNB systems.

Table 1 Electrical properties of $B_2N^{(-,0,+)}$ in ground and exited states, electric potential (EP) and isotropic Fermi contact couplings (MHz) (IFCC) for two position of BNB: 1—isolated and 2—non-isolated

State (*N_e)	$E_e(Hartree)$ Isolated BNB	All electron configuration (Total energy of $\|\alpha\rangle$* ($Homo-Lumo$)**	β electron configuration Total Energy of $\|\beta\rangle$* Beta virtual**	$r_e(B_1N)$ $r_e(NB_2)$ (*) in $B_{12}N_{12}$	A_1 (2, 1, 3, −2, −1) A_2 (2, 1, 3, −1, −2)	$B^{EP_1}-N^{EP_2}-B^{EP_3}$ *Dipole **IFCC (N, B_1, B_2) isolated	$B^{EP_1}-N^{EP_2}-B^{EP_3}$ *Dipole **IFCC (N,B_1,B_2) in $B_{12}N_{12}$ (non-isolated)
$\tilde{X}^2\Sigma^+$	−104.0781959[a]	$[A],\pi^4,\sigma^2,\sigma^1\|\alpha\rangle=-0.44641$[a]	$[B]\sigma^1\|\beta\rangle=-0.26180$[a]				
($C_{\infty v}$)	−104.0820328[a′]	$*E(\|\alpha\rangle)(-34.87083)$[a]	$*(-34.15046)$[a]				
(*17e)	−104.0754917[a″]	$**(-0.48614)$[a]	$**(-0.17697)$[a]				
$\tilde{X}^2\Sigma_u^+$	−104.0781959[b]	$[A']\pi_u^4,4\sigma_g^2,3\sigma_u^1\|\alpha\rangle=-0.44641$[b]	$[B'],4\sigma_g^1\|\beta\rangle=-0.26180$[b]	$*1.3198$[z]	$*A_1=180.0$[z]	$EP_1=EP_3=-11.37$[z]	$EP_1=EP_3=-11.31$[z]
($D_{\infty h}$)		$*(-34.87079)$[b]	$*(-34.15042)$[b]	$*1.3198$[z]	$*A_2=180.0$[z]	$EP_2=-18.34$[z]	$EP_2=-18.29$[z]
		$**(-0.48614)$[b]	$**(-0.17697)$[b]			*0.000	*1.4436
						**−28.3, 431.1, 431.1[z]	**−17.2, 738.8, 713.6[z]
$\tilde{X}^2\Sigma_u^+$	−103.6396773[d]	$[A']\pi_u^4,4\sigma_g^2,3\sigma_u^1\|\alpha\rangle=-0.42477$[d]	$[B'],4\sigma_g^1\|\beta\rangle=-0.24844$[d]	1.3176[d]	$A_1=180.0$[d]		
($D_{\infty h}$)		$*(-34.74888)$[d]	$*(-34.06924)$[d]	1.3176[d]	$A_2=180.0$[d]		
(*17e)		$**(-0.49245)$[d]	$**(-0.18742)$[d]				
$\tilde{X}^2\Sigma_u^+$	−104.159145[f]	$[A']\pi_u^4,4\sigma_g^2,3\sigma_u^1\|\alpha\rangle=-0.44701$[f]	$[B'],4\sigma_g^1\|\beta\rangle=-0.26341$	1.3275[f]	$A_1=180.0$[f]		
($D_{\infty h}$)	−104.1355512[n]	$*(-34.86501)$	$*(-34.14329)$	1.3275	$A_2=180.0$		
		$**(-0.48249)$	$**(-0.17779)$				
$\tilde{A}^2\Sigma_g^+$	−104.1047582[k]	$[A']\pi_u^4,4\sigma_g^1,3\sigma_u^2\|\alpha\rangle=-0.44638$[u]	$[A']\pi_u^4,4\sigma_u^1,=-0.26134$	1.3154[k]	$A_1=180.0$[k]		
(*17e)	−104.0781729[k′]	$*(-34.8744)$[u]	$*(-34.15408)$	1.3154[k]	$A_2=180.0$[k]		
		$**(-0.48626)$[u]	$**(-0.17666)$				
$\tilde{B}^4\Pi_g$	−104.0297022[h]	$[A']\pi_u^4,\pi_g^2,\sigma_g^1\|\alpha\rangle=-0.26899$[h]	$[A'],\pi_u^2\|\beta\rangle=-0.4965$[h]	$*1.3079$[x]	$*A_1=180.0$[x]	$EP_1=EP_3=-11.38$[x]	$EP_1=EP_3=-11.25$[x]
(*17e)	−104.0141196[a]	$*(-35.04484)$[h]	$*(-33.74801)$	$*1.3079$[x]	$*A_2=180.0$[x]	$EP_2=-18.35$[x]	$EP_2=-18.27$[x]
		$*(-0.30125)$[h]	$**(-0.50595)$			*0.00	*0.03
						**20.7, 404.1, 404.1[x]	**12.6, 410.5, 410.5[x]
$\tilde{X}^1\Sigma_g^+$	−104.1965676[a]	$[A']1\pi_u^4,4\sigma_g^2,3\sigma_u^2=-0.13904$[a]		$*1.335$[y]	$A_1=*180.0$[y]	$EP_1=EP_3=-11.63$[y]	$EP_1=EP_3=-11.44$[y]
(*18e)	−104.2019114[a′]	$*E(\|\alpha\rangle)=-32.48647$[a]		$*1.335$[y]	$A_2=*180.0$[y]	$EP_2=-18.6$[y]	$EP_2=-18.46$[y]
	−104.1950169[a″]	$**-0.36286$				*0.00	*0.02
$\tilde{X}^1\Sigma_g^+$	−104.1965676[b]	$*E(\|\alpha\rangle)=-32.48644$[b]		1.3291[b]	$A_1=180.0$[b]		
(*18e)				1.3291	$A_2=180.0$		
$\tilde{X}^1\Sigma_g^+$	−104.1145486[c]	$[A']\pi_u^4,\sigma_g^2,\sigma_u^2=-0.13454$[c]		1.3459[c]	$A_1=179.8967$[c]		
(*18e)	−104.1162881[c′]			1.3459[c]	$A_2=179.9181$[c]		
	−104.112568[c″]						
$\tilde{A}^3\Pi_u$	−104.0884685[a]	$[C]\pi_u^4,3\sigma_u^1,1\pi_g^1\|\alpha\rangle=-0.03986$[h]	$[C']\pi_u^4,4\sigma_g^1\|\beta\rangle=-0.01559$[h]	$*1.3422$[w]	$A_1=*180.0$[w]	$EP_1=EP_3=-11.67$[w]	$EP_1=EP_3=-11.49$[w]
(*18e)	−104.1164696[h]	$*E(\|\alpha\rangle)=-32.79721$[h]	$*E(\|\beta\rangle)=-32.26335$[h]	$*1.3422$	$A_2=*180.0$[w]	$EP_2=-18.60$[w]	$EP_2=-18.46$[w]
	−104.0809447[a′]	$**-0.25941$[h]	$**-0.14777$[h]			*0.000	*0.008
	−104.0792592[a″]					**−15.7, 208.2, 208.2	**−12.3, 266.3, 268.8
$\tilde{X}^1\Sigma_g^+$	−103.7454365[a]	$[D](1\pi_u^4),(4\sigma_g^2=-0.57788$[a])		1.2938[v]	$A_1=180.0$[v]	$EP_1=EP_3=-11.47$[v]	$EP_1=EP_3=-11.14$[v]
(*16e)	−103.8054934[a′]	$*E(\|\alpha\rangle)=-36.52419$[a]		1.2938[v]	$A_2=180.0$[v]	$EP_2=-18.45$[v]	$EP_2=-18.16$[v]
	−103.7545006[a″]	$**-0.17926$[a]				*0.000	*0.009
$\tilde{X}^1\Sigma_g^+$	−103.6023122[m]	$[D](1\pi_u^4),(4\sigma_g^2=-0.57803$[g])		1.3156[m]	$A_1=179.981$[m]		
(*16e)	−103.3012055[g]	$*E(\|\alpha\rangle)=-36.51985$[g]		1.3156[m]	$A_2=179.985$[m]		
	−103.8377401[f]	$**-0.17944$[g]		1.3003[h]			
	−103.7903312[h]			1.3004[h]			

Table 1 continued

State (*N_e)	$E_e(Hartree)$ Isolated BNB	All electron configuration (Total energy of $\|\alpha\rangle*$ $(Homo-Lumo)**$	β electron configuration Total Energy of $\|\beta\rangle*$ Beta virtual**	$r_e(B_1N)$ $r_e(NB_2)$ (*) in $B_{12}N_{12}$	A_1 $(2,1,3,-2,-1)$ A_2 $(2,1,3,-1,-2)$	$B^{EP_1}-N^{EP_2}-B^{EP_3}$ *Dipole **IFCC (N, B_1, B_2) isolated	$B^{EP_1}-N^{EP_2}-B^{EP_3}$ *Dipole **IFCC (N,B_1,B_2) in $B_{12}N_{12}$ (non-isolated)
$\tilde{B}^3\Sigma_g$ (*16e)	-103.7609202^{a} -103.7767141^{h} $-103.7628505^{a'}$ $-103.7590557^{a''}$	$\{[A']4\sigma_g^1, 3\sigma_u^1, \pi_u^4\}^{a}$ $\pi_u^2\|\alpha\rangle = -0.74323^{a}$ $*E(\|\alpha\rangle)(-37.33372)^{a}$ $**(-0.53385)^{a}$	$\{[A'], \pi_u^2\|\beta\rangle = -0.75222\}^{a}$ $*E(\|\beta\rangle)(-35.72475)^{a}$ $**(-0.52131)^{a}$	*1.2976[w] *1.2976[w]	A_1 = *180.0[w] A_2 = *180.0[w]	$EP_1 = EP_3 = -11.04^{w}$ $EP_2 = -18.07^{w}$ *0.000 {**}26.6, 592.5, 605.1	$EP_1 = EP_3 = -11.1^{w}$ $EP_2 = -18.11^{w}$ *0.2599 {**}26.6, 592.5, 605.1

[***A***]: $1\sigma^2, 2\sigma^2, 3\sigma^2, 4\sigma^2, 5\sigma^2$

[***A′***]: $1\sigma_g^2, 1\sigma_u^2, 2\sigma_g^2, 3\sigma_g^2, 2\sigma_u^2$

[***B***]: $\sigma^1, \sigma^1, \sigma^1, \sigma^1, \sigma^1, \pi^2$

[***B′***]: $1\sigma_g^1$, $2\sigma_g^1$, $1\sigma_u^1$, $3\sigma_g^1$, $2\sigma_u^1$, $1\pi_u^2$

[**C**]: $1\sigma_g^2, 1\sigma_u^2, 2\sigma_g^2, 3\sigma_g^2, 2\sigma_u^2, 4\sigma_g^2$

[**C′**]: $1\sigma_g, 1\sigma_u, 2\sigma_g, 3\sigma_g, 2\sigma_u$

[***D***]: $1\sigma_g^2$, $2\sigma_{g,}^2 1\sigma_u^2$, $3\sigma_g^2$, $2\sigma_u^2$

K′ TD/EPR-III//QCISD/EPR-III

[a] QCISD/EPR-III

[a′] MP_4D/EPR-III//QCISD/EPR-III

[a″] MP_4SDQ/EPR-III//QCISD/EPR-III

[b] QCISD/EPR-III ($\theta_{const} = 180.0$)

[c] QCISD/EPR-II

[c′] MP_4D/EPR-II//QCISD/EPR-II

[c″] MP_4SDQ/EPR-II//QCISD/EPR-II

[f] CBS-lq

[h] QCISD(T)/EPR-III

[k] TD/EPR-III//QCISD (T)/EPR-III

[d] CASSCF(11,12)/UHF

[m] CASSCF(10,12)/EPR-II

[g] CASSCF(10,12)ROHF AUG-cc-pvqz

[z] b3p86/6-31g*

[x] b3lyp/6-31g*

[y] m062x/epr-ii

[w] b3lyp/6-31g*

[v] CASSCF(11,12)/AUG-cc-pvqz

[n] CBS4O

[u] TD/EPR-II

Table 2 Energy of $B_2N^{(-,0,+)}$ in ground and exited states inside the $B_{12}N_{12}$ ring

StateE_e(Hartree) of BNB inside $B_{12}N_{12}$		All electron configuration $*$(Homo − Lumo)	β electron $r_e(B_1N), r_e(NB_2)$ $*$(Homo − Lumo) in $B_{12}N_{12}$	
Radical (*17e)				
$\tilde{X}^2\Sigma_u^+(D_{\infty h})$	-104.3253894^a	$[\boldsymbol{A}']\pi_u^4, 4\sigma_g^2, 3\sigma_u^1\|\alpha\rangle =$ $-0.32452^a * (-0.11397)^a$	$[\boldsymbol{B}'], 4\sigma_g^1\|\beta\rangle = -0.26180^a$ $*(-0.10659)^a$	$1.3206^a, -1.3206^a$ $\Delta = 0.00$
$\tilde{X}^2\Sigma^+(C_{\infty v})$	-104.3236681^a	$[\boldsymbol{A}], \pi^4, \sigma^2, \sigma^1\|\alpha\rangle =$ $-0.32764^a * (-0.11361)^a$	$[\boldsymbol{B}]\sigma^1\|\beta\rangle = -0.26180^a$ $*(-0.10711)^a$	$1.3406^a, -1.3206^a$ $\Delta = 0.02$
$\tilde{X}^2\Sigma_u^+(D_{\infty h})$	-104.709269^b	$[\boldsymbol{A}']\pi_u^4, 4\sigma_g^2, 3\sigma_u^1\|\alpha\rangle =$ $-0.29134^b * (-0.06778)^b$	$[\boldsymbol{B}'], 4\sigma_g^1\|\beta\rangle = -0.27320^a$ $**(-0.03864)^b$	$1.3198^b, -1.3198^b$ $\Delta = 0.00$
$\tilde{X}^2\Sigma^+(C_{\infty v})$	-104.7363847^b	$[\boldsymbol{A}], \pi^4, \sigma^2, \sigma^1\|\alpha\rangle =$ $-0.29698^b * (-0.08395)^b$	$[\boldsymbol{B}]\sigma^1\|\beta\rangle = -0.27855^b$ $*(-0.06184)^b$	$1.3398^b, -1.3198^b$ $\Delta = 0.02$
$\tilde{B}^4\Pi_g(D_{\infty h})$	-104.4168689^c	$[\boldsymbol{A}']\pi_u^4, \pi_{g,}^2\sigma_g^1\|\alpha\rangle = -0.24531^c$ $*(-0.05861)^c$	$[\boldsymbol{A}'], \pi_u^2\|\beta\rangle = -0.28057^c$ $*(-0.05587)^c$	$1.3079^c, -1.3079^c$ $\Delta = 0.00$
$\tilde{B}^4\Pi_g(C_{\infty v})$	-104.4160878^c	$[\boldsymbol{A}']\pi_u^4, \pi_{g,}^2\sigma_g^1\|\alpha\rangle =$ $-0.24517^c * (-0.05878)^c$	$[\boldsymbol{A}'], \pi_u^2\|\beta\rangle - 0.28057^c$ $*(-0.05587)^c$	$1.3279^c, -1.3079^c$ $\Delta = 0.02$
Anion(*18e)				
$\tilde{X}^1\Sigma_g^+$ $(D_{\infty h})$	-104.4992772^c	$[\boldsymbol{A}']\pi_u^4, \sigma_g^2, \sigma_u^2 = -0.16695^c$ $*(-0.08082)^c$		$1.335^c, -1.335^c$ $\Delta = 0.00$
$\tilde{X}^1\Sigma_g^+$ $(C_{\infty v})$	-104.4985276^c	$[\boldsymbol{A}']\pi_u^4, \sigma_g^2, \sigma_u^2 = -0.16712^c$ $*(-0.08038)^c$		$1.355^c, -1.335^c,$ $\Delta = 0.02$
$\tilde{A}^3\Pi_u$ $(D_{\infty h})$	-104.5794228^c	$[\mathbf{C}]\pi_u^4, 3\sigma_u^1, 1\pi_g^1\|\alpha\rangle = -0.08563^c$ $*(-0.06068)^e$	$[\boldsymbol{C}']\pi_{u,}^4, 4\sigma_g^1\|\beta\rangle = -0.0999^c$ $*(-0.0591)^c$	$1.3422^c, -1.3422^c$ $\Delta = 0.00$
$\tilde{A}^3\Pi_u$ $(C_{\infty v})$	-104.5777979^c	$[\mathbf{C}]\pi_u^4, 3\sigma_u^1, 1\pi_g^1\|\alpha\rangle = -0.08579^c$ $*(-0.06179)^c$	$[\boldsymbol{C}']\pi_{u,}^4, 4\sigma_g^1\|\beta\rangle = -0.1030^c$ $*(-0.05844)^c$	$1.3822^c, -1.3422^c$ $\Delta = 0.04$
Cation (*16e)				
$\tilde{X}^1\Sigma_g^+(D_{\infty h})$	-104.2335066^c	$[\mathbf{D}](1\pi_u^4), (4\sigma_g^2 = -0.46871^c)$ $*(-0.02983)^c$		$1.294^c, -1.294^c$ $\Delta = 0.00$
$\tilde{X}^1\Sigma_g^+$ $(C_{\infty v})$	-104.234079^c	$[\mathbf{D}](1\pi_u^4), (4\sigma_g^2 = -0.46856^c)$ $*(-0.02957)^c$		$1.304^c, -1.294^c$ $\Delta = 0.01$
$\tilde{B}^3\Sigma_g(D_{\infty h})$	-104.12761977^c	$\{[\boldsymbol{A}']4\sigma_g^1, 3\sigma_u^1, \pi_u^4, \}$ $\pi_u^2\|\alpha\rangle = -0.44236^c$ $*(-0.10744)^c$	$\{[\boldsymbol{A}'], \pi_u^2\|\beta\rangle = -0.43209\}^c$ $*(-0.04714^c$	$1.2976^c, -1.2976^c$ $\Delta = 0.00$
$\tilde{B}^3\Sigma_g(C_{\infty v})$	-104.1125986^c	$\{[\boldsymbol{A}']4\sigma_g^1, 3\sigma_u^1, \pi_u^4, \}$ $\pi_u^2\|\alpha\rangle = -0.45361^c$ $*(-0.11862)^c$	$\{[\boldsymbol{A}'], \pi_u^2\|\beta\rangle = -0.42857\}^c$ $*(-0.03399)^c$	$1.3376^c, -1.2976^c$ $\Delta = 0.04$

$[\boldsymbol{A}]$: $1\sigma^2, 2\sigma^2, 3\sigma^2, 4\sigma^2, 5\sigma^2$

$[\boldsymbol{A}']$: $1\sigma_g^2, 1\sigma_u^2, 2\sigma_g^2, 3\sigma_g^2, 2\sigma_u^2$

$[\boldsymbol{B}]$: $\sigma^1, \sigma^1, \sigma^1, \sigma^1, \sigma^1, \pi^2$

$[\boldsymbol{B}']$: $1\sigma_g^1, 2\sigma_g^1, 1\sigma_u^1, 3\sigma_g^1, 2\sigma_u^1, 1\pi_u^2$

$[\boldsymbol{C}]$: $1\sigma_g^2, 1\sigma_u^2, 2\sigma_g^2, 3\sigma_g^2, 2\sigma_u^2, 4\sigma_g^2$

$[\boldsymbol{C}']$: $1\sigma_g, 1\sigma_u, 2\sigma_g, 3\sigma_g, 2\sigma_u$

$[\boldsymbol{D}]$: $1\sigma_g^2, 2\sigma_{g,}^2 1\sigma_u^2, 3\sigma_g^2, 2\sigma_u^2$

[a] M062x/6-31g*

[b] B3p86/6-31g*

[c] B3LYP/6-31g*

[d] M062x/EPR-II

[e] B3p86/EPR-II

Table 3 Charges from ECP fitting for BNB in two position of isolated and external field of $B_{12}N_{12}$

State of BNB	BN bonds of $B_{12}N_{12}$	$\gamma = \frac{V_B - V_N}{r_{BN}}$	Force $= (\Sigma_x^2 + \Sigma_y^2 + \Sigma_y^2)^{\frac{1}{2}}$, θ = angle of force vector, $\delta(q_B - q_N)$ from ECP	$B^{\delta q_1}-N^{\delta q_2}-B^{\delta q_3}$ $\Delta = r_1(B_1N) - r_2(B_2N)$ "Isolated BNB" Charges from ESP fitting	$*B^{\delta q_1}-N^{\delta q_2}-B^{\delta q_3}$ and $\Delta = r_1(B_1N) - r_2(B_2N)$ Inside $B_{12}N_{12}$ Charges from ESP fitting
$\tilde{X}^2\Sigma_u^+$ Radical	B_2–N_1	$\gamma = 4.7184$[a]	$0.89, -38.18^\circ, 0.806$[a]	$\Delta^u = 0.0$ and $\delta q_1 = \delta q_3 = -0.055, \delta q_2 = 0.11$	$\Delta^u = 0.0$ and $\delta q_1 = \delta q_3 = 0.23, \delta q_2 = 0.52$
	B_3–N_4	$\gamma = 4.7168$[a]	$0.86, 53.92^\circ, 0.804$[a]	$\Delta^u = 0.02$ and $\delta q_1 = -0.15, \delta q_3 = 0.05, \delta q_2 = 0.10$	$\Delta^u = 0.02$ and $\delta q_1 = 0.24, \delta q_3 = 0.23, \delta q_2 = 0.52$
	B_6–N_5	$\gamma = 4.7191$[a]	$0.88, 55.22^\circ, 0.807$[a]	$\Delta^k = 0.0$ and $\delta q_1 = \delta q_3 = -0.08, \delta q_2 = 0.16$	$\Delta^k = 0.0$ and $\delta q_1 = -0.13, \delta q_3 = -0.14, \delta q_2 = 0.67$
	B_7–N_8	$\gamma = 4.7186$[a]	$0.93, -37.11^\circ, 0.806$[a]	$\Delta^k = 0.05$ and $\delta q_1 = -0.13, \delta q_3 = 0.02, \delta q_2 = 0.15$	$\Delta^k = 0.05$ and $\delta q_1 = 0.29, \delta q_3 = 0.98, \delta q_2 = 0.09$
				$\Delta^k = 0.07$ and $\delta q_1 = -0.13, \delta q_3 = 0.00, \delta q_2 = 0.13$	$\Delta^k = 0.07$ and $\delta q_1 = -0.2, \delta q_3 = -0.13, \delta q_2 = 0.66$
				$\Delta^y = 0.0$ and $\delta q_1 = \delta q_3 = -0.035, \delta q_2 = 0.07$	$\Delta^y = 0.0$ and $\delta q_1 = \delta q_3 = -0.3, \delta q_2 = 1.08$
				$\Delta^y = 0.05$ and $\delta q_1 = 0.05, \delta q_3 = -0.11, \delta q_2 = 0.06$	$\Delta^y = 0.05$ and $\delta q_1 = -0.63, \delta q_3 = -0.08, \delta q_2 = 1.17$
				$\Delta^y = 0.07$ and $\delta q_1 = 0.08, \delta q_3 = -0.14, \delta q_2 = 0.06$	$\Delta^y = 0.07$ and $\delta q_1 = 0.13, \delta q_3 = 0.00, \delta q_2 = 1.21$
$\tilde{X}^1\Sigma_g^+$	B_2–N_1	$\gamma = 4.6644$[a]	$1.28, 88.21^\circ, 0.232$	$\Delta^z = 0.0$ and $\delta q_1 = \delta q_3 = ?????, \delta q_2 = ???$	$\Delta^z = 0.0$ and $\delta q_1 = \delta q_3 = -0.76, \delta q_2 = 2.35$
Anion	B_3–N_4	$\gamma = 4.6630$[a]	$1.35, -3.39^\circ, 0.228$	$\Delta^z = 0.03$ and $\delta q_1 = -0.94, \delta q_3 = -1.0, \delta q_2 = 0.94$	$\Delta^z = 0.03$ and $\delta q_1 = -0.76, \delta q_3 = -0.72, \delta q_2 = 2.31$
	B_6–N_5	$\gamma = 4.6651$[a]	$1.23, 2.79^\circ, 0.232$	$\Delta^z = 0.05$ and $\delta q_1 = -0.91, \delta q_3 = -0.99, \delta q_2 = 0.90$	$\Delta^z = 0.05$ and $\delta q_1 = -0.78, \delta q_3 = -0.71, \delta q_2 = 2.32$
	B_7–N_8	$\gamma = 4.6649$[a]	$1.41, 89.59^\circ, 0.242$	$\Delta^z = 0.07$ and $\delta q_1 = -0.35, \delta q_3 = -0.37, \delta q_2 = -0.28$	$\Delta^z = 0.07$ and $\delta q_1 = -0.66, \delta q_3 = -0.42, \delta q_2 = 1.92$
				$\Delta^x = 0.0$ and $\delta q_1 = \delta q_3 = -?????, \delta q_2 = ???$	$\Delta^x = 0.0$ and $\delta q_1 = \delta q_3 = -1.1, \delta q_2 = 2.9$
				$\Delta^x = 0.05$ and $\delta q_1 = -0.87, \delta q_3 = -0.94, \delta q_2 = 0.81$	$\Delta^x = 0.05$ and $\delta q_1 = -1.04, \delta q_3 = -1.07, \delta q_2 = 2.83$
				$\Delta^x = 0.10$ and $\delta q_1 = -0.79, \delta q_3 = -0.94, \delta q_2 = 0.73$	$\Delta^x = 0.10$ and $\delta q_1 = -0.98, \delta q_3 = -1.04, \delta q_2 = 2.76$
				$\Delta^x = 0.14$ and $\delta q_1 = -0.73, \delta q_3 = -0.93, \delta q_2 = 0.66$	$\Delta^x = 0.14$ and $\delta q_1 = -0.93, \delta q_3 = -1.03, \delta q_2 = 2.70$
				$\Delta^x = 0.20$ and $\delta q_1 = -0.65, \delta q_3 = -0.92, \delta q_2 = 0.57$	$\Delta^x = 0.20$ and $\delta q_1 = -0.81, \delta q_3 = -0.96, \delta q_2 = 2.54$
$\tilde{X}^1\Sigma_g^+$				$\Delta^x = 0.01$ and $\delta q_1 = 0.79, \delta q_3 = 0.82, \delta q_2 = -0.61$	$\Delta^x = 0.01$ and $\delta q_1 = 0.29, \delta q_3 = 0.32, \delta q_2 = -0.43$
Cation				$\Delta^x = 0.03$ and $\delta q_1 = 0.76, \delta q_3 = 0.86, \delta q_2 = -0.62$	$\Delta^x = 0.03$ and $\delta q_1 = 0.27, \delta q_3 = 0.37, \delta q_2 = -0.47$
				$\Delta^x = 0.05$ and $\delta q_1 = 0.74, \delta q_3 = 0.89, \delta q_2 = -0.63$	$\Delta^x = 0.05$ and $\delta q_1 = 0.25, \delta q_3 = 0.40, \delta q_2 = -0.47$
				$\Delta^x = 0.08$ and $\delta q_1 = 0.69, \delta q_3 = 0.94, \delta q_2 = -0.63$	$\Delta^x = 0.08$ and $\delta q_1 = 0.23, \delta q_3 = 0.47, \delta q_2 = -0.51$

[a] QCISD/EPR-III

[u] m062x/6-31g*

[k] b3p86/6-31g*

[y] hf/epr-ii

[x] hf/6-31g*

[z] m062x/epr-ii

Table 4 Attraction and repulsion energies (eV) between $BNB^{(-,0,+)}$ and $B_{12}N_{12}$ ring in ground and exited states

$+\Delta = r_1(B_1N) - r_2(B_2N)$ $-\Delta = r_2(B_2N) - r_1(B_1N)$								$\Delta E^{\mathbf{A}ttraction(-)}_{Repulsion(+)}(eV) = E_t - (E_{B_{12}N_{12}} + E_{BNB})$							
								Ground state							
								$\tilde{X}^2\Sigma_u^+$ (Radical)				$\tilde{X}^1\Sigma_g^+$ (Anion)		$\tilde{X}^1\Sigma_g^+$ (Cation)	
$\pm\Delta^a$	$\pm\Delta^b$	$\pm\Delta^c$	$\pm\Delta^d$	$\pm\Delta^e$	$\pm\Delta^f$	$\pm\Delta^g$	$\pm\Delta^h$	ΔE^a	ΔE^b	ΔE^c	ΔE^d	ΔE^e	ΔE^f	ΔE^g	ΔE^h
0.000	0.000	0.00	0.00	0.00	0.00	0.00	0.00	−13.738	−13.988	−3.030	−1.701	−5.74	−2.711	0.239	0.881
0.005	0.01	0.01	0.01	0.01	0.01	0.01		−14.129	−14.400	−4.121	−1.680	−5.498	−2.705	0.246	
0.01	0.02	0.02	0.02	0.02	0.02	0.02		−14.146	−14.436	−3.776	−1.654	−5.511	−2.700	0.253	
0.02	0.03	0.03	0.03	0.03	0.03	0.03		−14.180	−14.472	−3.154	−1.623	−5.527	−2.698	0.260	
0.03	0.04	0.04	0.04	0.04	0.04	0.04		−14.215	−14.510	−3.145	−1.489	−5.543	−2.697	0.267	
0.035	0.05	0.05	0.05	0.05	0.05	0.05		−14.234	−14.549	−3.126	−1.457	−5.561	−2.699	0.274	
0.038	0.06	0.06		0.06	0.06	0.06		−14.245	−14.590	−3.863		−5.579	−2.688	0.282	
0.05	0.07	0.07		0.07	0.07	0.07		−14.291	−14.632	−4.003		−5.598	−2.709	0.289	
0.06	0.08	0.075		0.08	0.08			−14.331	−14.675	−4.002		−5.619	−2.700		
0.062	0.09	0.077		0.09				−14.339	−14.720	−3.377		−5.639			
0.065	0.091	0.08		0.10				−14.352	−14.725			−5.661			
0.067	0.092			0.12				−14.360	−13.688			−5.707			
0.07	0.095			0.14				−3.494	−13.689			−5.755			
0.075	0.10			0.17				−3.496	−13.690			−5.831			
	0.11			0.20					−13.692			−5.911			
	0.13			0.25					−13.698			−6.051			

$\pm\Delta^i$	$\pm\Delta^j$	$\pm\Delta^k$	Exited state		
			$\tilde{B}^4\Pi_g$ (Radical) ΔE^i	$\tilde{A}^3\Pi_u$ (Anion) ΔE^j	$\tilde{B}^3\Sigma_g$ (Cation) ΔE^k
0.00	0.00	0.00	−4.691	−7.634	−3.636
0.01	0.01	0.01	−4.686	−7.630	−3.638
0.02	0.04	0.04	−4.680	−7.623	−3.276
0.03	0.06	0.05	−4.674	−7.620	−3.285
0.05	0.08	0.06	−4.660	−7.618	−3.690
0.052	0.10	0.00	−4.658	−7.618	
0.055			−5.381		
0.06			−5.388		
0.09			−5.430		

[a] $UHF/EPR - II$ and $r_e = 1.3105$

[f] $M062x/epr - II$ and $r_e = 1.335$

[b] UHF/6–31g* and $r_e = 1.3089$

[g] $HF/6 - 31g*$ and $r_e = 1.302$

[c] B_3P86/6 - 31g* and $r_e = 1.3198$

[d] $M062x$/6 - 31g* and $r_e = 1.3206$

[e] HF/6 - 31g* and $r_e = 1.3371$

[h] $B3P86/epr - II//\text{CASSCF}(11,12)\text{rohf AUG} - \text{cc} - \text{pvqz}$, and $r_e = 1.294$

[i] $B3lyp/6 - 31g* //\text{qcisd(T)/epr} - \text{iii}$, and $r_e = 1.3079$

[j] $B3lyp/6 - 31g* //\text{qcisd}(T)/\text{epr} - iii$, and $r_e = 1.3422$

[k] $B3lyp/6 - 31g* //\text{qcisd}(T)/\text{epr} - iii$, and $r_e = 1.2976$

Table 5 The NBO, electric potential, anisotropic spin dipole couplings (ASDF), isotropic Fermi contact coupling {*IFCC*[$f(\Delta)$], *IFCC* [$f(\theta)$]}, atomic occupancies and Fock matrix data of isolated and non-isolated forms of $B_2N^{(-,0,+)}$ in ground and exited states

State (*N_e)	Isolated BNB (r_e = 1.3176) IFCC for nitrogen			ASDF of non-isolated BNB Baa, Bbb, Bcc	Hybrids coefficient	$E_{acceptor_{(j)}} - E_{Donor_{(i)}}$ *Fock matrix $\left(F_{i,j}, a.u.\right)$	Atomic occupancies*
	Δ and θ	IFCC $f(\Delta)$	IFCC $f(\theta)$				
$\tilde{X}^2\Sigma_u^+$	0.0, 0.0	−29.8	−29.8	N^f: −11.2, −9.4, 20.5	$\|\psi\rangle_{BD(1)} = 0.91SP_{N_1}^{1.01} + 0.41SP_{B_2}^{2.46^a}$	$\|\psi\rangle_{BD^*(2)} - \|\psi\rangle_{BD(1)} = 2.01$	$\|\alpha\rangle N : 2s^{0.77}2P_x^{0.84}2P_y^{0.84}2P_z^{0.87}$
(*17e)	0.02, 3.0	−29.1	−29.8	B^f: −24.0, −21.0, 45.0	$\|\psi\rangle_{BD(2)} = 0.96SP_{N_1}^{1.0} + 0.29SP_{B_2}^{1.0^a}$	*0.094	$\|\alpha\rangle B : 2s^{0.76}2P_x^{0.79}2P_y^{0.79}2P_z^{0.40}$
	0.04, 10.0	−26.6	−29.8	B^f: −22.6, −19.8, 42.4	$\|\psi\rangle_{BD(3)} = 0.96SP_{N_1}^{1.0} + 0.29SP_{B_2}^{1.0^a}$	$\|\psi\rangle_{BD^*(3)} - \|\psi\rangle_{BD(1)} = 1.00$	$\|\beta\rangle N : 2s^{0.80}2P_x^{0.86}2P_y^{0.86}2P_z^{0.83}$
	0.06, 20.0	−23.5	−29.9	N^g: −8.9, −8.9, 17.8	$\|\psi\rangle_{BD^*(1)} = 0.28SP_{N_1}^{1.0} - 0.95SP_{B_2}^{1.0^a}$	*0.089	$\|\beta\rangle B : 2s^{0.50}2P_x^{0.69}2P_y^{0.69}2P_z^{0.16}$
	0.08, 30.0	−20.5	−29.9	B^g: −21.6, −21.4, 42.9	$\|\psi\rangle_{BD^*(2)} = 0.42SP_{N_1}^{1.01} - 0.90SP_{B_3}^{0.95^a}$	$\|\psi\rangle_{BD^*(1)} - \|\psi\rangle_{BD(2)} = 0.7$	
	0.085, 40.0	−19.7	−29.6	B^g: −21.6, −21.4, 42.9	$\|\psi\rangle_{BD^*(3)} = 0.70SP_{B_2}^{0.97} - 0.70SP_{B_3}^{0.97^a}$	*0.029	
	0.086, 50.0	+4.35	−28.9				
$\tilde{X}^1\Sigma_g^+$					$\|\psi\rangle_{BD(1)} = 0.90SP_{N_1}^{1.01} + 0.43SP_{B_2}^{2.26^a}$	$\|\psi\rangle_{BD^*(3)} - \|\psi\rangle_{BD(1)} = 1.94$	$\|\alpha,\beta\rangle N : 2s^{1.59}2P_x^{1.70}2P_y^{1.70}2P_z^{1.66}$
(*18e)					$\|\psi\rangle_{BD(2)} = 0.66SP_{N_1}^{1.0} + 0.75SP_{B_2}^{1.0^a}$	*0.107	$\|\alpha,\beta\rangle B : 2s^{0.97}2P_x^{0.14}2P_y^{0.14}2P_z^{0.37}$
					$\|\psi\rangle_{BD(3)} = 0.95SP_{N_1}^{1.0} + 0.32SP_{B_2}^{1.0^a}$	$\|\psi\rangle_{BD^*(1)} - \|\psi\rangle_{BD(1)} = 0.73$	
					$\|\psi_{BD^*(1)} = 0.44SP_{N_1}^{1.01} - 0.90SP_{B_2}^{2.24^a}$	*0.021	
					$\|\psi\rangle_{BD^*(2)} = 0.75SP_{N_1}^{1.0} - 0.67SP_{B_3}^{1.0^a}$	$\|\psi\rangle_{BD^*(3)} - \|\psi\rangle_{BD(3)} = 1.94$	
					$\|\psi\rangle_{BD^*(3)} = 0.32SP_{N_1}^{1.0} - 0.94SP_{B_3}^{1.0^a}$	*0.107	
$\tilde{B}\ ^3\Sigma^+$				N^f: −10.5, 1.5, 9.0	$\|\psi\rangle_{BD(1)} = 0.90SP_{N_1}^{1.0} + 0.42SP_B^{0.72^b}$	$\|\psi\rangle_{BD^*(3)} - \|\psi\rangle_{BD(1)} = 1.98$	$\|\alpha\rangle N : 2s^{0.78}2P_x^{0.81}2P_y^{0.81}2P_z^{0.87}$
(*16e)				B^f: 26.3, − 22.1, 48.5	$\|\psi\rangle_{BD(2)} = 0.96SP_{N_1}^{1.0} + 0.26SP_B^{1.0^b}$	*0.119	$\|\alpha\rangle B : 2s^{0.72}2P_x^{0.92}2P_y^{0.92}2P_z^{0.44}$
				B^f: −27.4, −22.3, 49.8	$\|\psi\rangle_{BD(3)} = 0.96SP_{N_1}^{1.0} + 0.26SP_B^{1.0^b}$	$\|\psi\rangle_{BD^*(1)} - \|\psi\rangle_{BD(2)} = 0.77$	$\|\beta\rangle N : 2s^{0.77}2P_x^{0.87}2P_y^{0.87}2P_z^{0.86}$
					$\|\psi\rangle_{BD^*(1)} = 0.42SP_{N_1}^{1.0} - 0.90SP_{B_2}^{1.0^b}$	*0.028	$\|\beta\rangle B : 2s^{0.10}2P_x^{0.62}2P_y^{0.62}2P_z^{0.08}$
						$\|\psi\rangle_{BD^*(1)} - \|\psi\rangle_{BD(2)} = 0.7$	
						*0.029	
$\tilde{B}^4\Pi_g$	0.0, 0.0	20.26, −29.8					
(17e)	0.01, 0.0	20.26, −29.8					
	0.02, 0.0	20.27, −29.8					
	0.03, 0.0	20.28, −29.8					
	0.04, 0.0	20.30, −20.8					
	0.05, 0.0	20.30, −20.8					
	0.06, 0.0	20.44, −20.8					
	0.07, 0.0	20.50, −20.8					

Table 5 continued

State (*N_e)	Isolated BNB (r_e = 1.3176) IFCC for nitrogen		ASDF of non-isolated BNB	Hybrids coefficient	$E_{\text{acceptor}_{(j)}} - E_{\text{Donor}_{(i)}}$ *Fock matrix $(F_{ij}, a.u.)$	Atomic occupancies*
	Δ and θ	IFCC $f(\Delta)$	IFCC $f(\theta)$	Baa, Bbb, Bcc			
$\tilde{A}^3\Pi_u$ (*18e)			N[f]: −10.7, −10.6, 21.3	$\lvert\psi\rangle_{BD(1)} = 0.91SP^{1.0}_{N_1} + 0.40SP^{1.62^h}_{B_2}$	$\lvert\psi\rangle_{BD^*(3)} - \lvert\psi\rangle_{BD(1)} = 1.94$	$\lvert\alpha\rangle$N : $2s^{0.75}2p^{0.81}_x 2p^{0.60}_y 2p^{0.86}_z$
			B[f]: −15.5, −15.0, 30.5	$\lvert\psi\rangle_{BD(2)} = 0.97SP^{1.0}_{N_1} + 0.26SP^{1.0^h}_{B_2}$	*0.107	$\lvert\alpha\rangle$B : $2s^{0.74}2p^{0.09}_x 2p^{0.70}_y 2p^{0.43}_z$
			B[f]: −15.6, −15.1, 30.6	$\lvert\psi\rangle_{BD(3)} = 0.91SP^{1.0}_{N_1} + 0.40SP^{1.62^h}_{B_3}$	$\lvert\psi\rangle_{BD^*(4)} - \lvert\psi\rangle_{BD(1)} = 1.01$	$\lvert\beta\rangle$N : $2s^{0.80}2p^{0.87}_x 2p^{0.90}_y 2p^{0.86}_z$
				$\lvert\psi\rangle_{BD(4)} = 0.70SP^{0.51}_{B_2} + 0.70SP^{0.51}_{B_3}$	*0.064	$\lvert\beta\rangle$B : $2s^{0.46}2p^{0.06}_x 2p^{0.04}_y 2p^{0.16}_z$
				$\lvert\psi\rangle_{BD^*(1)} = 0.45P^{1.0}_{N_1} - 0.91SP^{1.62^h}_{B_2}$	$\lvert\psi\rangle_{BD^*(1)} - \lvert\psi\rangle_{BD(2)} = 0.73$	
				$\lvert\psi\rangle_{BD^*(2)} = 0.26SP^{1.0}_{N_1} - 0.97SP^{1.0^h}_{B_3}$	*0.021	
				$\lvert\psi\rangle_{BD^*(3)} = 0.40SP^{1.0}_{N_1} - 0.91SP^{1.62^h}_{B_3}$		
				$\lvert\psi\rangle_{BD^*(4)} = 0.70SP^{0.51}_{B_2} - 0.70SP^{05^{1h}}_{B_3}$		

[a] QCISD/EPR-III

[h] QCISD(T)/EPR-III

[f] b3lyp/6-31g*(pop = ChelpG)

[g] m062x/6-31g* pop = ChelpG

The failure of B3LYP and most of the other popular functional to correctly describe medium range of exchange and correlation energies limits their applicability for distant non-bonded systems (our non-bonded system has a short distance). Moreover, some recent studies have shown that inaccuracy for the medium-range exchange energies leads to large systematic errors in the prediction of molecular properties [46–50].

Although DFT methods incorrectly underestimated the second-order Jahn–Teller distortion for isolated BNB (which led the B3LYP calculations to predict a symmetric structure with too much frequency for anti-symmetric stretch in contrast to "UHF" solution for the ground state [51]), they work well for the $BN^{(-,0,+)}B$–$B_{12}N_{12}$ systems and they work very well with the estimated second-order Jahn–Teller for BNB (Table 3; Fig. 4).

As it can be observed in Table 4, the results of m062x including epr-ii and 6-31g* basis sets, compared to other functionals such as B3P86 and B3LYP, have different values (in lower level), though it is in the same way and identical changing. In both of two major DFT methods (m062x and B3LYP), the results show an attraction for $BN^{(-,0)}B$ and a repulsion for $BN^{(+)}B$ with $B_{12}N_{12}$ ring.

In Table 1, the difference between the two positions of global minima and local minima of isolated BNB for both $|\alpha\rangle$ and $|\beta\rangle$ is 8.77 cm^{-1}. It is indicated in our calculations that the total energies for both of them are the same (i.e., −104.0781959). This is due to the fact that the spin orbital energies are related to the small bending angles of A_1 and A_2, which have an extremely low bending frequency of 70 cm^{-1}. Harmonic frequencies were determined at the QCISD/EPR-III//prop = epr and characterized by 228.79 cm^{-1} ($\vartheta_1 = \vartheta_1'$, bending mode "$\pi_u$"), 1178.64 cm^{-1} (ϑ_2, symmetric stretching "σ_g") and 2146.42 (ϑ_3, asymmetric stretching "σ_u"). The IR and Raman intensities for ϑ_3 are 10165.0 and 0.00, respectively, while the "ϑ_2" mode has intensity in Raman (51.0), but zero intensity in IR region.

As it is indicated in Tables 1 and 2, the energy of $\tilde{X}^2\sum_u^+$ in the state of $|\alpha\rangle = -0.44641$ for isolated $BNB^{(0)}$ is higher than that of $|\alpha\rangle = -0.32452$ for non-isolated $BNB^{(0)}$ as well as the one for $|\beta\rangle = -0.26341 > -0.26180$ is too. The energies of $\tilde{B}^4\Pi_g$ can be shown as:

$$|\alpha\rangle_{\text{isolated}} = -0.26899 > |\alpha\rangle_{\text{non-isolated}} = -0.24517 \qquad (14)$$

and

$$|\beta\rangle_{\text{isolated}} = -0.4965 > |\beta\rangle_{\text{non-isolated}} = -0.28057 \qquad (15)$$

Therefore, as it is observed, the difference between two situations in $|\beta\rangle$ is significantly higher than that of $|\alpha\rangle$ and with a higher stability of the isolated $\tilde{B}^4\Pi_g$ compared to the non-isolated systems. Furthermore, $|\alpha\rangle$ orbital energy is

Table 6 Isotropic Fermi contact coupling (IFCC) of $B_2N^{(0)}$ in ground ($\tilde{X}^2\Sigma_u^+$) and exited ($\tilde{B}^4\Pi_g$) states

State (*N_e)	$\Delta = r_2 - r_1$ $\theta_{cons} = 180.0$	IFCC[$f(\Delta)$] N, B_1, B_2	$\Delta\theta = \theta_1 - \theta_1$ $r_{cons} = 1.3176$	$IFCC[f(\theta)]$ N, B_1, B_2
$\tilde{X}^2\Sigma_u^+$ (*17e)	$\Delta = 0.000$	−29.81, 428.6, 428.6	$\Delta\theta = 0.0$	−29.81, 428.6, 428.6
	Δ= 0.010	−29.76, 386.2, 469.7	$\Delta\theta = 2.0$	−29.81, 428.71, 428.71
	$\Delta = 0.020$	−29.11, 348.2, 508.1	$\Delta\theta = 3.0$	−29.81, 428.77, 428.77
	$\Delta = 0.030$	−28.02, 316.1, 541.9	$\Delta\theta = 5.0$	−29.81, 428.95, 428.95
	$\Delta = 0.040$	−26.64, 290.3, 570.2	$\Delta\theta = 10.0$	−29.83, 429.84, 429.84
	$\Delta = 0.050$	−25.12, 270.7, 592.6	$\Delta\theta = 20.0$	−29.87, 433.44, 433.44
	$\Delta = 0.060$	−23.54, 256.7, 609.5	$\Delta\theta = 30.0$	−29.86, 439.68, 439.68
	$\Delta = 0.070$	−21.98, 247.6, 621.3	$\Delta\theta = 40.0$	−29.61, 448.75, 448.75
	$\Delta = 0.080$	−20.46, 242.7, 628.7	$\Delta\theta = 50.0$	−28.85, 460.82, 460.82
	$\Delta = 0.082$	−20.10, 242.1, 629.8	$\Delta\theta = 60.0$	−27.16, 475.86, 475.86
	$\Delta = 0.085$	−19.72, 241.6, 630.9	$\Delta\theta = 70.0$	−24.06, 493.31, 493.31
	$\Delta = 0.086$	4.35, 60.3, 899.9	$\Delta\theta = 80.0$	−18.57, 512.55, 512.55
	$\Delta = 0.087$	4.46, 59.4, 901.2	$\Delta\theta = 90.0$	−10.65, 533.75, 533.75
	$\Delta = 0.090$	4.79, 56.6, 904.7		
$\tilde{B}^4\Pi_g$	$\Delta = 0.000$	20.26, 377.8, 377.8		
	$\Delta = 0.010$	20.26, 381.2, 377.9		
	$\Delta = 0.020$	20.26, 384.5, 377.9		
	$\Delta = 0.030$	20.28, 387.8, 377.9		
	$\Delta = 0.040$	20.30, 391.2, 377.9		
	$\Delta = 0.050$	20.30, 394.4, 377.9		
	$\Delta = 0.060$	20.38, 397.8, 377.9		
	$\Delta = 0.070$	20.44, 401.0, 377.8		
	$\Delta = 0.080$	20.50, 404.27, 377.7		

much more stable in an isolated system compared to that of the non-isolated system for cation and anion forms.

The energies of $|\alpha\rangle$ and $|\beta\rangle$ valance occupied MOs for the first triplet exited state $(1\sigma_g^2, 1\sigma_u^2, 2\sigma_g^2, 3\sigma_g^2, 2\sigma_u^2, 4\sigma_g^2, 1\pi_u^4, 4\sigma_u^1, 1\pi_g^1)$ are $1\pi_g^1|\alpha\rangle = -0.03986$, $4\sigma_u^1|\alpha\rangle = -0.23701$ and $\{1\pi_u^2|\alpha\rangle = -0.25466, -0.25136\}$, while those for $|\beta$ are $\{1\pi_u^2|\beta\rangle = -0.28802, -0.27730\}$, and $4\sigma_g^2|\beta\rangle = -0.01559$. The total energy of $|\alpha\rangle$ is higher than the total energy of $|\beta\rangle$, indicating stronger correlation in anion form compared to the other two forms of $B_2N^{(+,0)}$.

However, the unrestricted QCISD (T) wave function is considerably spin contaminated and characterized by a large T_1 value. The $\tilde{A}^3\Sigma_g^+$ excited state corresponding to the promotion of an electron from the highest occupied molecular orbital (HOMO), $3\sigma_u$ to the $4\sigma_u$ MO is predicted to be considerably above the $\tilde{A}^3\Pi_u$ state.

As it is shown in Table 1, the energy difference between the two states of $(\tilde{A}^2\Sigma_g^+)$ and $(\tilde{X}^2\sum_u^+)$ $\{(k-a)$ and $(k-k^{'})\}$ is 5829.75 and 5834.79 cm^{-1}, respectively. Those values are close to photoelectron spectroscopy calculations carried out by Asmis et al. [2]. He has argued that the signal observed in the 355 and 266 nm photoelectron spectra of B_2N^- indicates a photo detachment from the $(\tilde{X}^1\sum_g^+)$ to the ground and lowest excited state of neutral B_2N [i.e., $(\tilde{X}^2\sum_u^+)$ and $(\tilde{A}^2\sum_g^+)$ with a linear symmetry, assigned to the $\tilde{X}^1\sum_g^+ \rightarrow \tilde{X}^2\sum_u^+ + e^-$ and $\tilde{X}^1\sum_g^+ \rightarrow \tilde{A}^2\sum_g^+ + e^-$ transitions where the energy (T_0) of the term $(\tilde{A}^2\sum_g^+)$ is 0.785 eV or 6331.77 cm^{-1}) [2].

It is notable that the orbital binding of "$1\pi_u$" is a combination of all $2p_\pi$ orbitals on all three atoms of BNB, while "$4\sigma_g^2$" and "$3\sigma_u^1$" orbitals are close and not having any strong binding characteristic. The small separation of these two orbitals accounts for the small energy required to promote the molecule from the ground state to the first exited state at 5829.75 cm^{-1}. The difference between $(k-a)$ and $(k-k^{'})$ is $\approx$5 cm^{-1}, which is near 8.77 cm^{-1} (different between $C_{2V}/C_{\infty V}$ and $C_{\infty V}/D_{\infty h}$). In addition, $\tilde{B}^2\Pi_g$ (exited state above the$\tilde{A}^2\Sigma_g^+$) is subject to the Renner–Teller effect, leading to a complicated pattern of bending vibrational levels.

The data illustrated in Tables 1 and 4 indicate the photo detachment mechanism from the $(\tilde{X}^1\sum_g^+)$ to the ground and lowest excited states, which is confirmed for BNB

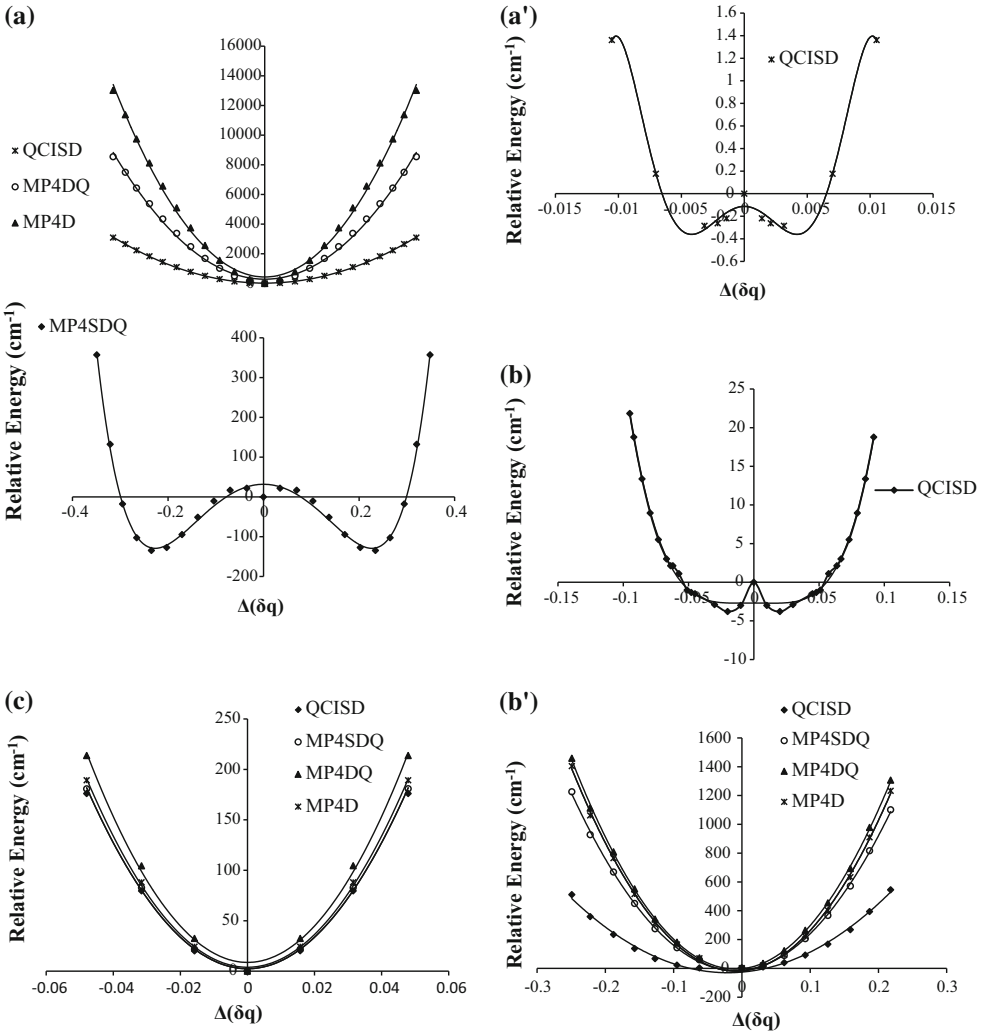

Fig. 1 The $B_2N^{(-,0,+)}$ relative energies versus B–N–B bond distance in various levels of theory, **a**, **a′** for cation, **b**, **b′** for radical and **c** for anion

radical in $B_{12}N_{12}$ field in neutral B_2N $\{(\tilde{X}^2\sum_u^+)$ and $(\tilde{A}^2\sum_g^+)\}$, though, in a high energy level.

It is notable that the electron configuration sequence for $|\alpha\rangle$ and $|\beta\rangle$ situations is not the same (Table 1). These sequences correspond to $[A']$ and $[B']$ for $|\alpha\rangle$ and $|\beta\rangle$, respectively, which result in the sequences of "$1\sigma_g > 1\sigma_u > 2\sigma_g$" for $|\alpha\rangle$ and "$1\sigma_g > 2\sigma_g > 1\sigma_u$" for $|\beta\rangle$.

The results of our calculations indicate the existence of a larger gap between $3\sigma_u$ and $1\pi_g$ orbitals both in isolated and in non-isolated $BN^{(0)}$ B, thereby placing the transition to $[\mathbf{A}']\pi_u^4, 4\sigma_g^2, 1\pi_g^1$ with the state of $\tilde{B}^2\Pi_g$ being much higher in energy. Analysis of the vibronic structure of $\tilde{B}^2\Pi_g - (\tilde{X}^2\sum_u^+)$ band system shows the transition to $\tilde{B}^2\Pi_g$ at 19452 cm^{-1}. However, the non-bonding characteristic of $1\pi_g$ and $3\sigma_u$ orbitals suggests no important changes in B–N bond length in this transition, as it is observed in the study carried out by Ding et al. [52]. Therefore, in spite of $\tilde{A}^2\sum_g^+$, the "$\tilde{B}^2\Pi_g$" excited configuration does contribute to the ground state wave function as a subject of Renner–Teller effect.

We have reinvestigated the anion form at the QCISD (T), QCISD, CCSD (T), MP4SDQ, MP4D and full space CASSCF levels of theory employing the triple zeta Aug-CC-PVTZ and EPR-III basis sets. Even though the cyclic B_2N^- anion structure cannot be predicted to lie above the $\tilde{X}^1\sum_g^+$ ground state in our calculations, it is notable that the lowest stable bent solution for $B_2N^{(-)}$ should be a $^3B_2$ state and not a singlet state.

4.3 Calculation of physical properties

The electrical properties in ground and exited states as well as the electrostatic potential (EP), geometry of BNB, Homo–Lumo gap and isotropic Fermi contact couplings (MHz) in two situations of (1) isolated BNB and (2) BNB under an external field of $B_{12}N_{12}$ (non-isolated) are listed in Tables 1 and 2. In addition, charges from ESP fitting,

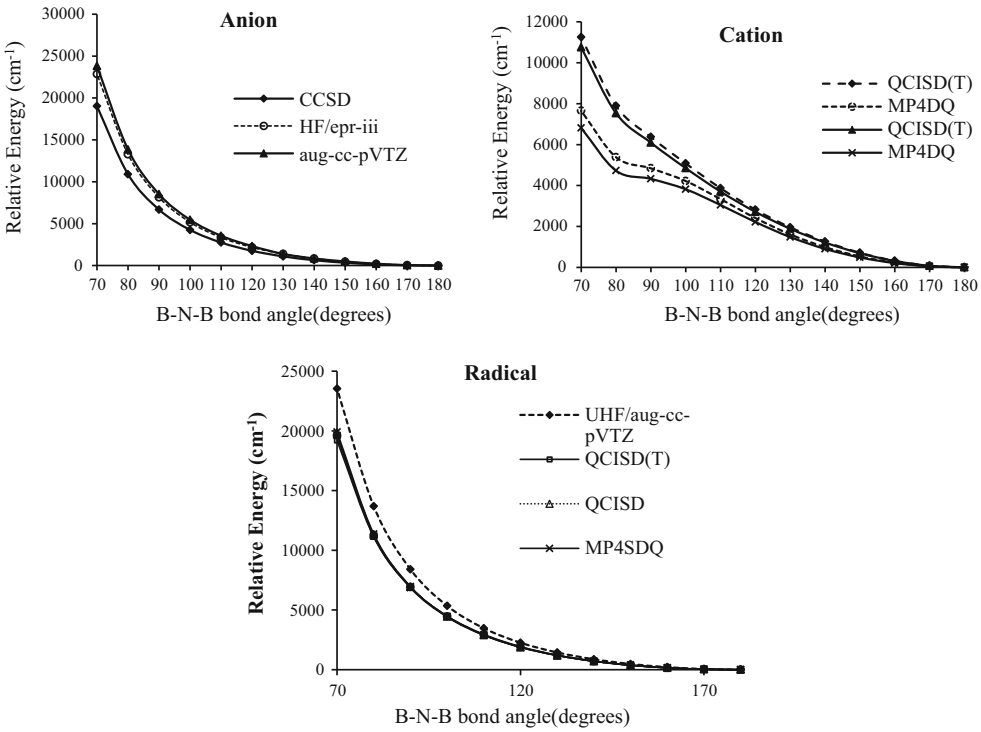

Fig. 2 Relative energies of $B_2N^{(-,0,+)}$ versus B–N–B bond angle in various levels of theory

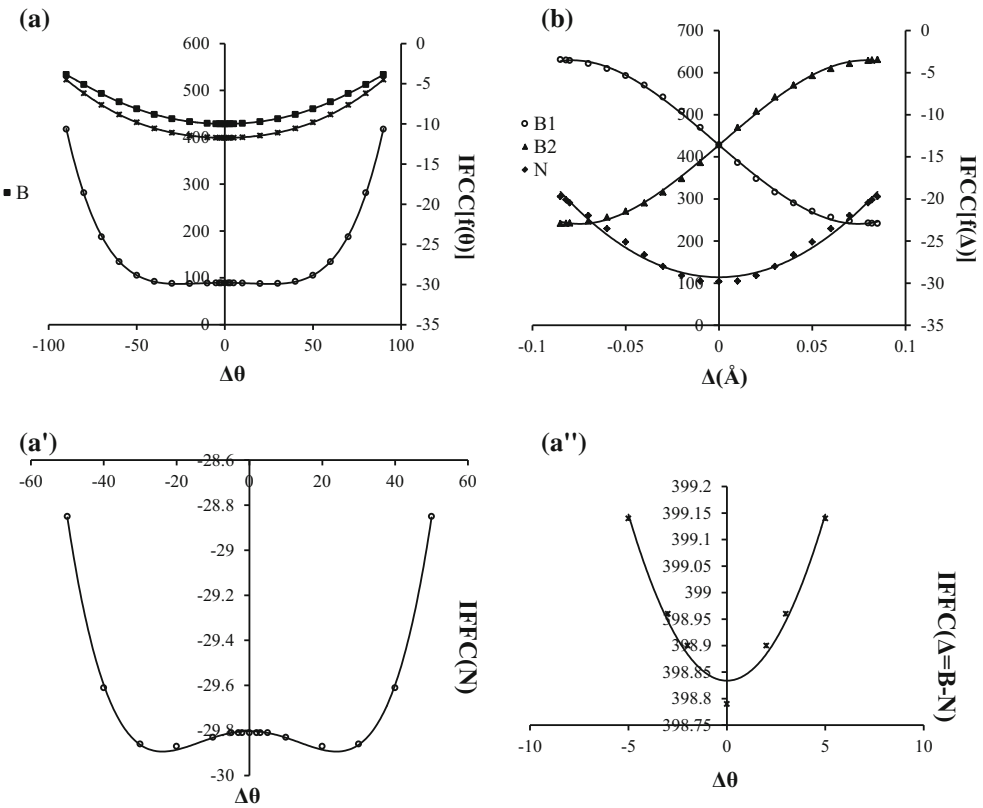

Fig. 3 Isotropic Fermi contact coupling (IFCC) of $B_2N^{(0)}$: **a** function of angles changing, **b** function of distances changing. The axes for nitrogen and borons have different scales, **a′** IFCC for N in a short scale between −30 and −29.8 indicates of IFCC breaking and **a″** different IFCC of B and N in a short scale

forces, $\gamma = (V_B - V_N)/r_{BN}$, attraction and repulsion energies (eV) between $BNB^{(-,0,+)}$ and $B_{12}N_{12}$ ring in ground and exited states are listed in Tables 3 and 4. Anisotropic spin dipole coupling (MHZ), the differences of $\left(E_{\text{acceptor}_{(j)}} - E_{\text{Donor}_{(i)}}\right)$ and NBO properties are listed in Table 5.

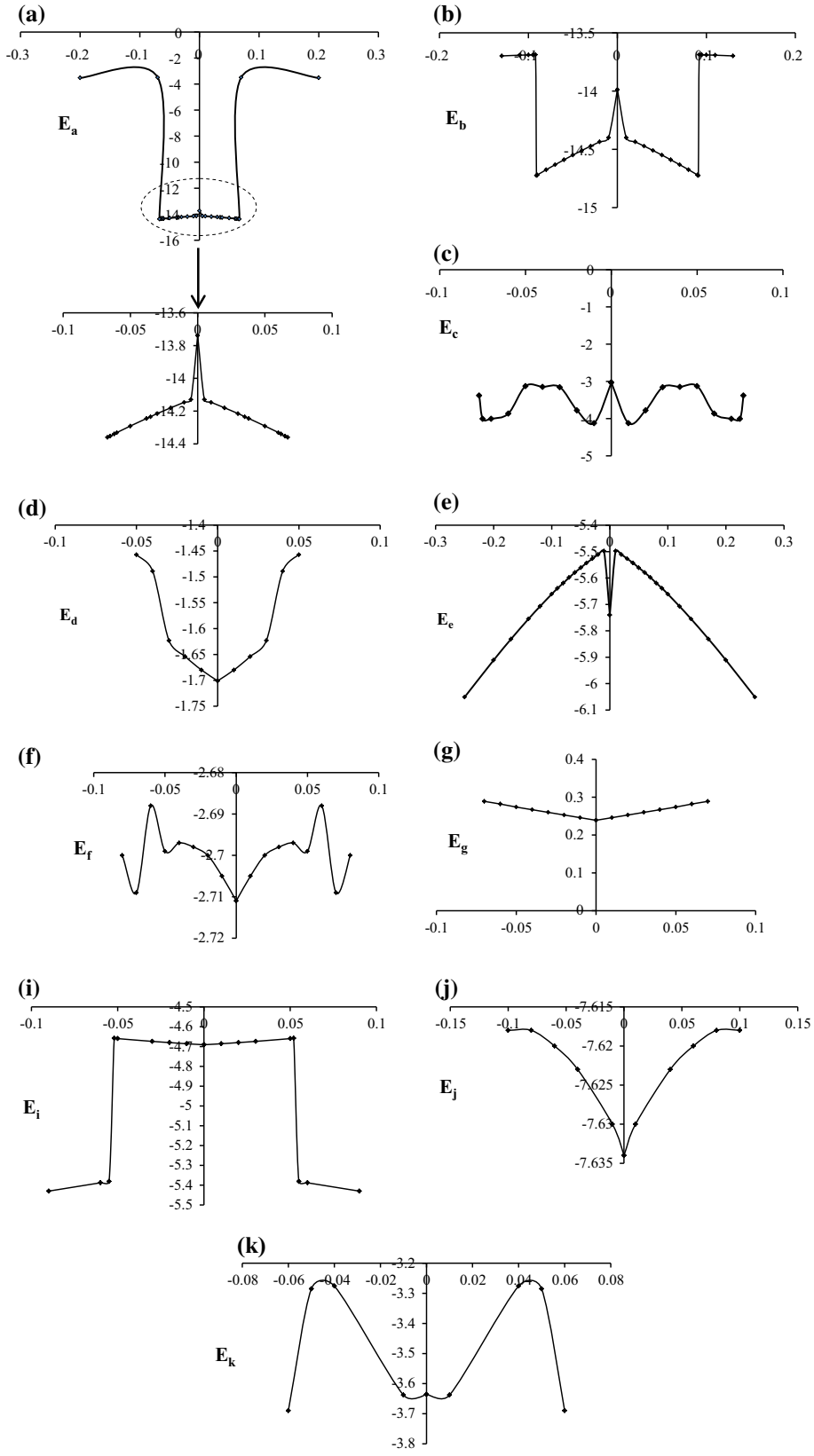

Fig. 4 The $B_2N^{(-,0,+)}$ relative energies versus B–N–B bond distance in various levels of theory for a non-isolated system in the BNB–$B_{12}N_{12}$ from Table 4 where (**a**–**d**) are for $\tilde{X}^2\Sigma_u^+$ (radical); **e**, **f** are for $\tilde{X}^1\Sigma_g^+$ (anion); **h** is for $\tilde{X}^1\Sigma_g^+$; and **i**–**k** are for $\tilde{B}^4\Pi_g$ (radical), $\tilde{A}^3\Pi_u$ (anion) and $\tilde{B}\ ^3\Sigma_g$ (cation), respectively

As it is indicated in Table 1, as opposed to the quantity of IFCC, the change of EP between the two situations of isolated and non-isolated BNB is rather small. In other words, the EP is not under the influence of the external field caused by the ring, while the IFCC is.

In addition, the dipole moment of radical $\tilde{X}^2\sum_u^+(D_{\infty h})$ from 0.000 (for an isolated BNB) to 1.4436 (for a non-isolated BNB) has been changed and the IFCC has been varied considerably between these two situations as well.

The charges of MESP fitting for isolated BNB radical and the summation of partial charges for two boron and one nitrogen ($B^{\delta q_1}-N^{\delta q_2}-B^{\delta q_3}$) in all items of the ranges from $\Delta = 0.0$ up to $\Delta = 0.07$ are zero (indicating a radical system) (Table 3).

Interestingly, the summation of partial charges in $B^{\delta q_1}-N^{\delta q_2}-B^{\delta q_3}$ for BNB radical inside the $B_{12}N_{12}$ is not zero, and it has been changed according to: $(0.23 + 0.23 + 0.52 = 0.98)$ for $\Delta^u = 0.0$, $(0.24 + 0.23 + 0.52 = 0.99)$ for $\Delta^u = 0.02$ and so on (Table 3). The difference between Δ^u, Δ^k and Δ^y is because of using various methods and basis sets; however, it is certain that the summation of partial charges in BNB radical in the external filed of $B_{12}N_{12}$ is far from zero and varies between 0.5 and 0.99. It could be due to the fact that the unpaired electron of nitrogen is localized while the BNB is under the influence of the external field of $B_{12}N_{12}$ or in another view that might happen due to either a poor choice of the method to evaluate atomic charges or a significant charge transfer between BNB and $B_{12}N_{12}$.

It is notable that in the interaction between $B_{12}N_{12}$ and BNB, there is more stability in $B_{12}N_{12}$ structure compared to the BNB structure due to the fact that the "γ" of the four bonds of $B_{12}N_{12}$ (B_2–N_1, B_3–N_4, B_6–N_5 and B_7–N_8) (around 4.71), the parameter of $\delta(q_B - q_N)$ (around 0.8), and the vector forces on these bonds (around $\approx$ 0.9) are identical (Table 3). Therefore, the most change in the isolated BNB compared to non-isolated system is related to the external field of $B_{12}N_{12}$. For the exited state of radical forms, even though the change in MESP for both the exited state($\tilde{B}^4\Pi_g$) and ground state $\left(\tilde{X}^2\sum_u^+\right)$ is negligible, as opposed to the ground state ($S = 1$ of BNB radical), the IFCC is not considerable for $S = 3/2$ (Table 1).

Table 3 illustrates the charges from MESP fitting for isolated anion. The sum of partial charges (in $B^{\delta q_1}-N^{\delta q_2}-B^{\delta q_3}$) for all items from $\Delta = 0.0$ to $\Delta = 0.2$ is -1 (indicating an anion form); however, the total partial charges of $B^{\delta q_1}-N^{\delta q_2}-B^{\delta q_3}$ for BNB anion inside the $B_{12}N_{12}$ are not -1, and they have been changed from $(-0.76 - 0.76 + 2.35 = 0.83)$ for $\Delta^z = 0.0$ to $(-0.66 - 0.42 + 1.92 = 0.84)$ for $\Delta^z = 0.07$ and (0.77) for $\Delta^x = 0.2$. As a result, the total partial charges for all the items of $BN^{(-)}B$ are positive (in contrast to isolated anion). It is due to the fact that the unpaired electron of nitrogen is localized while the BNB is under the influence of the external field of $B_{12}N_{12}$. It seems that the anion isolated in the field of $B_{12}N_{12}$ has changed to a radical form.

The parameters of "γ" for four bonds of $B_{12}N_{12}$, ($B_2 - N_1, B_3 - N_4, B_6 - N_5$ and $B_7 - N_8$ (around 4.66)), the $\delta(q_B - q_N)$ (around 0.23) and vector forces on these bonds (around $\approx$ 1.28–1.41) are given in Table 3, indicating that the interaction between BNB and $B_{12}N_{12}$ system in anion form is stronger than the radical form. These results are also further clarified in Table 2, illustrating the interaction energy and the energy of non-isolated BNB compared to that of isolated state of BNB. These results have shown that the stability sequences are: $\{BNB^{(-)} > BNB^{(0)} > BNB^{(+)}$ for non-isolated$\} \gg \{BNB^{(+)} > BNB^{(0)} > BNB^{(-)}$ for isolated$\}$.

Using Gaussian distribution of partial charges ranging from $\Delta^x = 0.0$ to $\Delta^x = 0.06$, the expectation values of charges were calculated, resulting in 0.21, 0.82 and 0.65 for cation, anion and radical, respectively. The nitrogen in non-isolated ground state of BNB is always positive for radical and anion and negative for cation, while in exited states, the sum of partial atomic charges is positive for all three forms. This charge distribution of nitrogen is the main reason of attraction for $B_2N^{(-,0)}$ and repulsion for $B_2N^{(+)}$ in the $B_{12}N_{12}$.

Harmonic frequencies were determined at the QCISD/EPR-III//prop = EPR level of theory and characterized by 224.70 cm^{-1}($\vartheta_1 = \vartheta_1'$, bending mode "$\pi_u$"), 1203.42 cm^{-1} (ϑ_2, symmetric stretching "σ_g") and 1837.50 (ϑ_3, asymmetric stretching "σ_u"). The IR and Raman intensities for ϑ_3 are 1494.6 and 0.00, respectively, while the "ϑ_2" mode has intensity in Raman (39.97) but zero intensity in IR region. The valence orbital occupancy of ground state $(\tilde{X}^1\sum_g^+)$ is: $1\sigma_g^2, 1\sigma_u^2, 2\sigma_g^2, 3\sigma_g^2, 2\sigma_u^2, 1\pi_u^4, 4\sigma_g^2, 3\sigma_u^2$, while the lowest excited triplet state in the $D_{\infty h}$ representation for anion form has been calculated (Table 1) and is predicted to be a $\tilde{A}^3\Pi_u$ state, lying at 2.94 eV $\{(\tilde{A}^3\Pi_u(a) - \tilde{X}^1\sum_g^+(a))$ in Table 1$\}$ which is above the $\tilde{X}^1\Sigma_g^+$ state (with the calculated value of 2.7 eV anion with photoelectron spectroscopy of $B_2N^{(-)}$).

A total of 4516 points have been used for fitting the atomic charges to electrostatic potential, and the charges of ESP in this fitting are: $\{N = 0.891292$, $B = -0.945425$, $B = -0.945867\}$. The nitrogen atom is always positive, while the two boron atoms are always negative which is appeared conversely for the $B_2N^{(+)}$. In the latter, the nitrogen in cation is negative and two borons are positive in all ESP calculations. Both the highest occupied molecular orbitals are predominantly non-bonding with the electron density being localized mainly on the "terminal" boron atoms.

Isotropic Fermi contact coupling (IFCC) of $B_2N^{(0)}$ as a function of angles and distances is shown in Table 6 and Fig. 3. Although the symmetry breaking cannot be seen in the IFCC $\{f(\Delta r)\}$, it can be seen in the IFCC $\{f(\Delta\theta)\}$ for the nitrogen in range of angles between $\Delta\theta = [50, -50]$ (Fig. 3a′). On the other hand, the SB has not been observed for the $\Delta(\Delta\theta) = \Delta\theta_B - \Delta\theta_N$ in the range of $\Delta\theta = [5, -5]$ (Fig. 3a). It seems that the nitrogen in SB problem plays a major role, which depends on a symmetry bond changing and angle deformation interaction $(\pi_u + \sigma_u)$.

As it is illustrated in Table 5, the results of NBO calculation indicate that the $2s_N$ orbital is considered to be primarily core-like, forming the $3\sigma_g$ orbital, though some mixing of the $2s_N$ orbital into the other σ_g orbitals is of course expected. The NBO analysis of the orbital containing the unpaired electron in BNB shows that most of the spin density is placed on boron's *sp* orbitals. The boron atomic orbitals are best explained as a "*sp*" hybrid, directed away from the nitrogen atom; however, they are bonding with consideration of the σP orbital on the nitrogen atom. The $2\sigma_u$ orbital is a bonding combination of the $2p\sigma$ orbital on the central nitrogen atom with $2sp\sigma$ hybrid orbitals on the two borons.

The anisotropic spin dipole coupling (ASDC) has been calculated for non-isolated form of BNB for $\tilde{X}^2\sum_u^+$, $\tilde{B}^3\Sigma^+$ and $\tilde{A}^3\Pi_u$ (Table 5). The data indicate that the ASDC (Baa) and ASDC (Bbb) are negative for all states as well as methods (except the Bbb for nitrogen in $\tilde{B}^3\Sigma^+$ which is a exited state of cation form); however, the ASDC (Bcc) is positive and its amount for two borons in different methods and states is approximately equal. However, it has been significantly changed for nitrogen, indicating that the character of nitrogen is much more important than two borons in $B_{12}N_{12}$–BNB non-covalent interaction.

The hyperfine parameters were calculated for the linear geometry with a bond length of 1.3176 Å using a CASSCF optimization at several levels of configuration interaction and exited states (Tables 5, 6; Fig. 3). A_{iso} in ground state for boron atoms varies, i.e., from 428.6 MHz at $\Delta = 0.0$ to 241.6 MHz at $\Delta = 0.085$ for B_1 and from 428.6 MHz at $\Delta = 0.0$ to 630.9 MHz at $\Delta = 0.085$ for B_2 (Fig. 3), while the Nitrogen A_{iso} varies smoothly from −29.8 MHz ($\Delta = 0.0$) to −19.7 MHz ($\Delta = 0.085$) (Tables 5, 6).

There is a critical point for A_{iso}(both in B and N) between $\Delta = 0.085$ and $\Delta = 0.086$ where the data reverse to 4.35 for N (Table 6), indicating the symmetry breaking in point charges or distances in this region. The dipolar hyperfine coupling constants exhibited negligible dependence on bond. The highest occupied orbital containing the unpaired electron is σ_u orbital with the most of the electron density on the boron atoms. Symmetry constrains this orbital to have only "σP" orbital contributions from nitrogen with no "s" character so that the isotropic hyperfine parameter from nitrogen would be small and arise mostly from spin polarization effects.

The molecular isotropic hyperfine(A_{iso}) values for BNB can be obtained from the experimental "$A_{||}$" and "$A_{\perp}$" using Eq. 14 [4]:

$$A_{iso} = \frac{(2A_{\perp} + A_{||})}{3} = \frac{8\pi}{3} g_e g_N \beta_e \beta_N \langle\delta(r)\rangle. \quad (16)$$

As a result, the experimental data are $B_1 = B_2 = 451$ and $N = -14.0$, which are in good agreement with our calculated results. Isotropic hyperfine interaction including "**g**" tensor for BNB shows a large boron isotropic amount. Thus, the properties of the g tensor eliminate the possibility of a low exited $^2\Pi_g$ state for the radical [4]. The averaged vibrations of B–N bond lengths, i.e., $IFCC[f(\Delta)]$ or $IFCC[f(\theta)]$, indicate that the ground state is precisely linear, quasi-linear or the geometry at the potential minimum went through a symmetry breaking to form a $C_{\infty v}$ structure. The reason of high symmetry breaking in a non-covalent reaction is mainly nitrogen atom. Furthermore, the partial charges on nitrogen cause repulsion or attraction between BNB and $B_{12}N_{12}$ systems of $BN^{(+)}B$ and $BN^{(-,0)}B$, respectively.

All in all, the nuclear hyperfine of various states is shown in Table 6 and Fig. 3. The nitrogen and one of the boron atoms in $\tilde{B}^4\Pi_g$ state are independent of "Δ" during hyperfine coupling calculation. Although these two states ($\tilde{B}^4\Pi_g$ and ground state) can interact along the anti-symmetric stretching as a reason of SB problem in BNB radical, the lack of the "correct" per-mutational symmetry of the wave functions which is arisen due to the oversimplification of the wave function is a major reason for spontaneous symmetry breaking. In this study, we have focused on the charge distribution of boron and nitrogen atoms to exhibit the charge breaking (Tables 1, 4).

As it is shown in Fig. 3, the symmetry breaking in point charge distribution not only indicates a barrier energy in the regions of 100–160 cm^{-1} [9, 51] or 20 cm^{-1} [53], but it also creates several SB through the asymmetry stretching (or interaction between asymmetry stretching and bending) with different barrier energies from high to small values for both isolated and non-isolated systems (Fig. 4). Therefore, the symmetry breaking barrier has a dynamic changing with no centro-symmetric form, and it only depends on the wave function or charge distribution. Furthermore, a large barrier can be estimated via fixed-node diffusion Monte Carlo methods in which $D_{\infty h}$ and $C_{\infty v}$ ROHF WFs (with

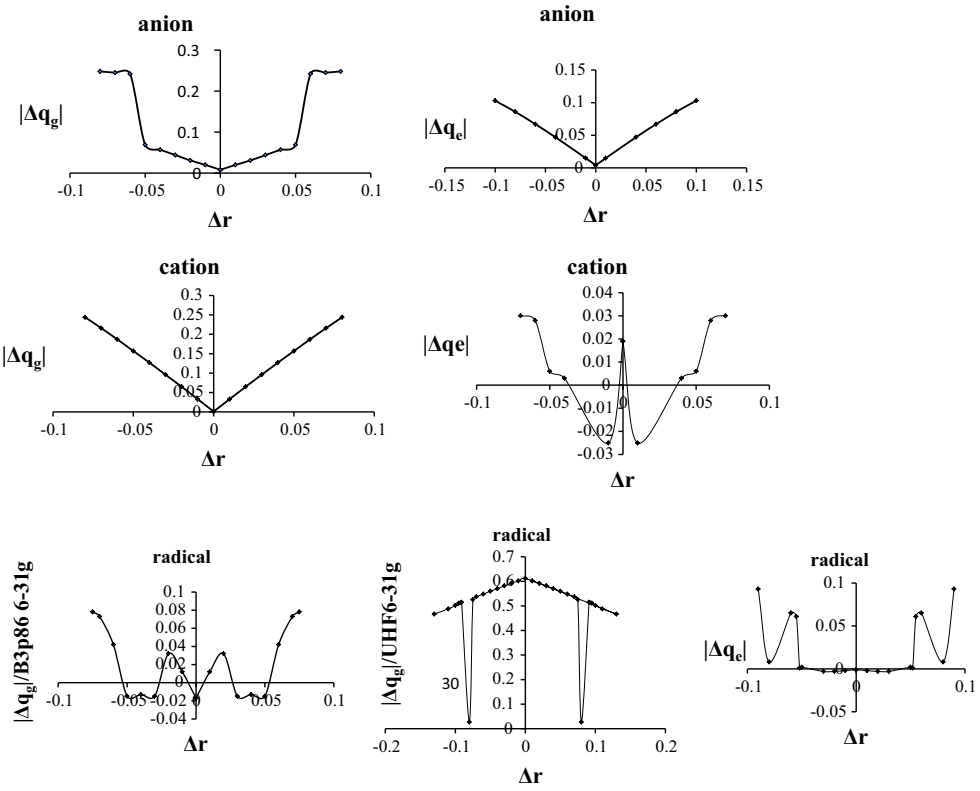

Fig. 5 The nitrogen charges versus the B–N–B bond distance in various levels of theory for a non-isolated system of BNB–$B_{12}N_{12}$

symmetric stretching) have energies separated by a gap as big as approximately 0.5 millihartree [54].

In this work, symmetry breaking occurs a few times in non-bonded isolated form of BNB (Fig. 4) as well as the $\tilde{X}^2\Sigma^+$ state (Table 4 and Fig. 4a, b). There is a breaking with 0.4 eV (around 15 mili hartree), which is 30 times more than the isolated system explained by Al-Saidi (i.e., around 0.5 mili hartree) [54]. This breaking for anion $\tilde{X}^1\sum_g^+$ happens four times with different values (Fig. 4f, k) (which is double for the exited state of $\tilde{B}^4\Pi_g$ is two times). The charges versus B–N changing and stretching are shown in Fig. 5, which clearly indicates the symmetry breaking in a non-isolated system in terms of charge distribution and wave function.

Due to the interaction of $B_{12}N_{12}$–BNB and SB dipole effect, the BNB radical has the highest dipole moment, while it is the lowest for anion form. Along with the high values of Θ, ϕ, the r of dipole moment holds a Gaussian distribution, which can be observed in the plotted Gaussian graphs of dipole moment (r) versus Θ and ϕ angles [14]. Based on our previous study in which the expectation values of $<\Delta E>$ have been obtained for radical, cation and anion of $BH_2N^{(-,0,+)}BH_2$ [14, 16], it seems that the r component of dipole moment, voltage differences and relative energies of the system in this study are quantized, and the system undergoes quantization through rotation.

5 Conclusion

The results of this study made it pretty clear that the SB problem is not a real phenomenon; it is a hidden function depending on various variables such as charge distribution, bond length, IFCC, Gaussian primitives, trial wave function properties and most importantly, external field of B_nN_n rings. It is indicated that the SB is generally applied to the electronic wave function failure in order to be transformed as an irreducible representation of the molecular point group, and thus, the failure of the electronic wave function is purely artifactual. It is not wise to conclude that only the special level of theory on the symmetry breaking for BNB is real (which has been concluded in Ref. [9]) due to the existence of some hidden variables in the electronic wave functions which should be considered.

Although the total wave functions of each molecule for Φ_n^{BNB} and $\Phi_m^{\mathrm{B_{12}N_{12}}}$ under permutation of electron coordinates are anti-symmetric, the product states of these non-bonded molecules under intermolecular exchange of the electrons cannot be anti-symmetric. Therefore, when the two B–N bonds are asymmetrically stretched, the "$4\sigma_g^2$" and "$3\sigma_u^1$" orbitals cannot be degenerate. On the other hand, there are major problems for introducing the inter-molecular anti-symmetrizer, because the anti-symmetrized unperturbed states are no longer eigen-functions of $H^{(0)}$, which follows the non-commutation $[\tilde{A}, H^{(0)}] \neq 0$. In other

words $\tilde{A}^{\mathrm{BNB-B_{12}N_{12}B}}\Phi_n^{\mathrm{BNB}}\Phi_m^{\mathrm{B_{12}N_{12}}}$ become linearly dependent and the choice of a linear independent subset would not be apparent. As it was mentioned, in the interaction between $B_{12}N_{12}$ and BNB the structure of $B_{12}N_{12}$ does not change when $+\Delta = r_1(B_1N) - r_2(B_2N)$ and $-\Delta = r_2(B_2N) - r_1(B_1N)$ have changed from $\Delta = 0.0$ to $\Delta = 0.1$ (Table 3). However, the energy of BNB has been changed significantly due to this asymmetry stretching mode.

We have figured that the symmetry breaking (SB) in an external field of B_nN_n which is caused due to some hidden variables not only exhibits an energy barrier, but it also creates several SBs through the asymmetry stretching with bending mode interaction. It is indicated in this study that the stability sequences of the BNB–$B_{12}N_{12}$ are: $\{BNB^{(-)} > BNB^{(0)} > BNB^{(+)}$ for non-isolated system$\} \gg \{BNB^{(+)} > BNB^{(0)} > BNB^{(-)}$ for isolated system$\}$. These kinds of systems could undergo transitions among different quantized levels and yield a spectrum in IR region with three rotational frequencies ($\vartheta_{\mathrm{radical-cation}}, \vartheta_{radical-anion}$, and $\vartheta_{\mathrm{anion-cation}}$).

References

1. Martin JML, François J-P, Gijbels R (1989) J Chem Phys 90:6469
2. Asmis KR, Taylor TR, Neumark DM (1999) J Chem Phys 111:8838
3. Martin JML, François J-P, Gijbels R (1990) Chem Phys Lett 172:354
4. Knight LB Jr, Hill DW, Kirk TJ, Arrington CA (1992) J Phys Chem 96:555
5. Martin JML, François J-P, Gijbels R (1992) Chem Phys Lett 193:243
6. Hassanzadeh P, Andrews L (1992) J Phys Chem 96:9177
7. Andrews L, Hassanzadeh P, Burkholder TR, Martin JML (1993) J Chem Phys 98:922
8. Thompson CA, Andrews L (1995) J Am Chem Soc 117:10125
9. Li X, Paldus J (2007) J Chem Phys 126:224304
10. Martin JML, El-Yazal J, François J-P, Gijbels R (1995) Mol Phys 85:527
11. Meloni G, Sai Baba M, Gingerich A (2000) J Chem Phys 113:8995
12. Graham WRK, Weltner W (1976) J Chem Phys 65:1516
13. Monajjemi M (2013) Chem Phys 425:29–45
14. Monajjemi M, Lee VS, Khaleghian M, Honarparvar B, Mollaamin F (2010) J Phys Chem C 114:15315
15. Monajjemi M, Boggs JE (2013) J Phys Chem A 117:1670
16. Monajjemi M (2012) Struct Chem 23:551
17. Walsh AD (1953) J Chem Soc 2260–2266. doi:10.1039/JR9530002260
18. London F (1930) Z Phys 63:245
19. Eisenschitz R, London F (1930) Z Phys 60:491
20. Physik Z (1937) Chemie 33:8–26
21. Szalewicz K, Jeziorski B (1995) In: Scheiner S (ed) *Molecular theory of gases and liquids*. Wiley, Chichester. ISBN 0-471-95921-9
22. Hirschfelder O, Curtiss CF, Bird RB (1954) *Molecular theory of gases and liquids*. Wiley, New York
23. Stone AJ (1996) The Theory of Intermolecular Forces. Clarendon Press, Oxford
24. Pyykkö P, Wang C, Straka M, Vaara J (2007) Phys Chem Chem Phys 9:2954–2958
25. Wang C, Pyykkö P, Straka M (2010) Phys Chem Chem Phys 12:6187–6203
26. Lennard-Jones JE (1931) Proc Phys Soc (London) 43:461
27. Edmonds AR (1957) *Angular momentum in quantum mechanics*. Princeton University Press, Princeton
28. Thompson WJ (1994) *Angular momentum*. Wiley, New York
29. Thorne KS (1980) Rev Mod Phys 52(2):299
30. Brink DM, Satchler GR (1968) Angular momentum, 2nd edn. Clarendon Press, Oxford
31. Barone V (1996) In: Chong DP (ed) Recent advances in density functional methods, Parts I. World Scientific Publ. Co
32. Chopra NG, Luyken RJ, Cherrey K, Crespi VH, Cohen ML, Louie SG, Zettl A (1995) Science 269:966
33. Blasé X, Rubio A, Louie SG, Cohen ML (1994) Europhys Lett 28L:335
34. Blasé X, Charlier JC, de Vita A, Car R (1997) Appl Phys Lett 70:197
35. Walker TEH, Richards WG (1970) J Chem Phys 52:1311
36. Koseki S, Schmidt MW, Gordon MS (1992) J Phys Chem 96:10768
37. Pople JA, Head-Gordon M, Raghavachari K (1987) J Chem Phys 87:5968
38. Bader RFW (1990) Atoms in molecule: a quantum theory. Oxford Univ. Press, Oxford
39. Besler BH, Merz KM, Kollman PA (1990) J Comput Chem 11:431
40. Chirlian LE, Francl MM (1987) J Comp Chem 8:894
41. Brneman CM, Wiberg KB (1990) J Comp Chem 11:361
42. Martin F, Zipse H (2005) J Comp Chem 26:97–105
43. Frisch MJ, Trucks GW, Schlegel HB, Scusera GE, Robb MA, Cheeseman JR, Zakrzewski VG, Montgomery JA, Stratmann RE, Burant JC, Dapprich S, Millam JM, Daniels AD, Kudin KN, Strain MC, Farkas O, Tomasi J, Barone V, Cossi M, Cammi R, Mennucci B, Pomelli C, Adamo C, Clifford S, Ochterski J, Petersson GA, Ayala PY, Cui Q, Morokuma K, Malick DK, Rabuck AD, Raghavachari K, Foresman JB, Cioslowski J, Ortiz JV, Baboul AG, Stefanov BB, Liu G, Liashenko A, Piskorz P, Komaromi I, Gomperts R, Martin RL, Fox DJ, Keith T, Al-Laham MA, Peng CY, Nanayakkara A, Gonzalez C, Challacombe M, Gill PMW, Johnson B, Chen W, Wong MW, Andres JL, Gonzalez C, Head-Gordon M, Replogle ES, Pople JA (1998) Gaussian 98, revision A 7. Gaussian Inc, Pittsburgh
44. Zhao Yan, Truhlar Donald G (2008) Theor Chem Acc 120:215–241
45. Zhao Yan, Truhlar Donald G (2008) Acc Chem Res 41(2):157–167
46. Check CE, Gilbert TM (2005) J Org Chem 70:9828–9834
47. Grimme SS (2006) Angew Chem Int Ed 45:4460–4464
48. Wodrich MD, Corminboeuf C, Schleyer PVR (2006) Org Lett 8:3631–3634
49. Schreiner PR, Fokin AA, Pascal RA Jr, de Meijere A (2006) Org Lett 8:3635–3638
50. Zhao Y, Truhlar DG (2006) Org Lett 8:5753–5755
51. Gwaltney SR, Head-Gordon M (2001) Phys Chem Chem Phys 3:4495
52. Ding H, Morse MD, Apetrei C, Chacaga L, Aier JP (2006) J Chem Phys 125:194315
53. Liu Y, Zou W, Bersuker IB, Boggs JE (2009) J Chem Phys 130:184305
54. Al-Saidi WA (2012) Chem Phys Lett 543:41–44